Higher-order epistasis within Pol II trigger loop haplotypes

Authors: Bingbing Duan[1], Chenxi Qiu[2], Steve W. Lockless[3], Sing-Hoi Sze[4,5], Craig D. Kaplan[1*]

Affiliations:

[1] Department of Biological Sciences, University of Pittsburgh, Pittsburgh, PA 15260.

[2] Department of Genetics, Harvard Medical School, Boston, MA 02215.

[3] Department of Biology, Texas A&M University, College Station, TX 77843.

[4] Department of Computer Science & Engineering, Texas A&M University, College Station, TX 77843.

[5] Department of Biochemistry & Biophysics, Texas A&M University, College Station, TX 77843.

Contact information: craig.kaplan@pitt.edu

Key words: trigger loop, haplotypes, epistasis, deep mutational scanning

ABSTRACT

RNA polymerase II (Pol II) has a highly conserved domain, the trigger loop (TL), that controls transcription fidelity and speed. We previously probed pairwise genetic interactions between residues within and surrounding the TL for the purpose of understand functional interactions between residues and to understand how individual mutants might alter TL function. We identified widespread incompatibility between TLs of different species when placed in the *Saccharomyces cerevisiae* Pol II context, indicating species-specific interactions between otherwise highly conserved TLs and its surroundings. These interactions represent epistasis between TL residues and the rest of Pol II. We sought to understand why certain TL sequences are incompatible with *S. cerevisiae* Pol II and to dissect the nature of genetic interactions within multiply substituted TLs as a window on higher order epistasis in this system. We identified both positive and negative higher-order residue interactions within example TL haplotypes. Intricate higher-order epistasis formed by TL residues was sometimes only apparent from analysis of intermediate genotypes, emphasizing complexity of epistatic interactions. Furthermore, we distinguished TL substitutions with distinct classes of epistatic patterns, suggesting specific TL residues that potentially influence TL evolution. Our examples of complex residue interactions suggest possible pathways for epistasis to facilitate Pol II evolution.

INTRODUCTION

Functional interactions among amino acid residues within a protein can be detected by genetic interactions in the form of epistasis. Epistasis between residues can dmodulate the phenotypic effects of mutations. Specific substitutions can create or relax functional constraints on the identity of residues at other positions in a protein, and impact evolutionary trajectories (MANI *et al.* 2008; PHILLIPS 2008; STARR AND THORNTON 2016; DOMINGO *et al.* 2019; PARK *et al.* 2022; JOHNSON *et al.* 2023; METZGER *et al.* 2023). Epistasis is the modulation, positive or negative, of the effect of one mutant by the presence of other mutants. This phenotypic modulation can be detected by observing differences in the phenotype of a double mutant from that expected from the cumulative effects of the two corresponding single mutants, which is the baseline expectation in the absence of epistasis (PHILLIPS 1998; HILL *et al.* 2008; MANI *et al.* 2008; PHILLIPS 2008). Prior studies found many epistatic interactions at both lower-orders (i.e. among residue pairs) and higher-orders (among many residue combinations). Higher-order epistasis, emerging from particular residues, can reflect specific biological or physical interactions and imply crucial roles of these residues in proteins' function and evolution (MELAMED *et al.* 2013; OLSON *et al.* 2014; BANK *et al.* 2015; POKUSAEVA *et al.* 2019; REDDY AND DESAI 2021; BAKERLEE *et al.* 2022; DING *et al.* 2022; LIN *et al.* 2022). In this work, we dissect complex higher-order epistasis by deep mutational scanning within an ultra-conserved and crucial active site domain, the trigger loop (TL), of RNA polymerase II (Pol II).

Pol II transcribes eukaryotic DNA into mRNA using an iterative nucleotide addition cycle (NAC) (BAR-NAHUM *et al.* 2005; WANG *et al.* 2006; MALINEN *et al.* 2012; DANGKULWANICH *et al.* 2013; KAPLAN 2013; KULDELL AND KAPLAN 2024). The TL is a critical domain for the NAC, and participates in all three steps: nucleotide selection, catalysis, and likely translocation by switching between different conformations (WANG *et al.* 2006; FOUQUEAU *et al.* 2013; BARNES *et al.* 2015). In each NAC, a matched substrate entering the active site induces or captures a conformational change of the TL from an open, catalysis-disfavoring state to a closed, catalysis-favoring state. Thus, the TL functions in kinetic selection to distinguish matched NTPs complementary to the DNA template from mismatched ones (WANG *et al.* 2006; HUANG *et al.* 2010; MALINEN *et al.* 2012; KAPLAN 2013; WANG *et al.* 2013; XU *et al.* 2014; BARNES *et al.* 2015). Full closure of the TL promotes catalysis (VASSYLYEV *et al.* 2007; WANG *et al.* 2013). Following

catalysis, the TL transits from the closed to the open state, facilitating polymerase translocation for the subsequent NAC (SEIBOLD *et al.* 2010; DA *et al.* 2012; LIU *et al.* 2016) (**Fig. 1A**). Additional TL conformations have been associated with other RNA polymerase activities such as pausing and backtracking (WANG *et al.* 2009; ZHANG *et al.* 2010; CHEUNG AND CRAMER 2011; MOSAEI AND ZENKIN 2021). With these transitions, the mobile TL balances transcription fidelity and speed (WANG *et al.* 2006; KAPLAN *et al.* 2008; KIREEVA *et al.* 2008; SYDOW *et al.* 2009; KAPLAN 2010; YUZENKOVA *et al.* 2010; LARSON *et al.* 2012; UNARTA *et al.* 2023; KULDELL AND KAPLAN 2024).

How do residues within the TL interact with each other to ensure its proper transition? Our observations of distinct pairwise interactions suggest that TL function is maintained by residue interaction networks (DUAN *et al.* 2023). For example, previous biochemical and genetic studies found mutations in the TL can modify its folding or dynamics, causing changes in catalytic activity. These changes include increases to catalytic rate, leading to faster elongation than WT in vitro (gain of function, GOF) or decreases to catalytic rate, leading to slower elongation than WT in vitro (loss of function, LOF) (KAPLAN *et al.* 2008; KIREEVA *et al.* 2008; KAPLAN *et al.* 2012; BRABERG *et al.* 2013; NAYAK *et al.* 2013; WINDGASSEN *et al.* 2014; BARNES *et al.* 2015; QIU *et al.* 2016). Our prior work on TL double mutants, including combinations between or within GOF and LOF mutations, identified distinct types of pairwise interactions. These interactions resulted in fitness levels that were either better or worse than expected, based on the simple assumption that independently functioning substitutions would have cumulative effects. This indicates that mutations interact in ways that alter fitness beyond the additive effects. These interactions include suppression, commonly observed in certain GOF/LOF combinations, which leads to better than expected fitness. The suppressive interactions support a model where single mutants act independently within double mutants. In this model, the effects are balanced in double mutants that consist of mutations with opposite effects. However, in some GOF/LOF combinations, we observed a lack of suppression, known as sign epistasis, indicating the effect of one mutant is controlled by the identity of another residue. In contrast, in double mutants with similar phenotypes (GOF/GOF or LOF/LOF), the effects are enhanced to a level that is similar or even beyond the additivity. This latter situation is known as synthetic sickness or lethality. However, we also observed a lack of enhancement for some GOF/GOF or LOF/LOF combinations, referred to as epistasis, revealing dependency between residues (KAPLAN *et al.* 2012; QIU *et al.* 2016; QIU AND KAPLAN 2019; DUAN *et al.* 2023).

The TL is highly conserved across evolution, supporting the idea that identities of key residues are highly constrained (PALO *et al.* 2021). Given this conservation, it was surprising that analogous mutations in a highly conserved residue yielded opposite effects in the conserved yeast Pol I and Pol II enzymes (VIKTOROVSKAYA *et al.* 2013). Given the TL's flexible and mobile character, along with its high conservation of sequence and function, it was an open question of if the TL is functionally self-contained, or evolutionary coupling through non-conserved residues is necessary to maintain its ability to achieve different conformations. Our recent studies identified widespread incompatibility between trigger loops of different species or enzymes placed into the yeast Pol II context, supporting the idea of an epistasis network from residues outside the TL is prominent in contributing to TL function and creating different contingencies for its evolution (DUAN *et al.* 2023). We wished to understand the drivers of this incompatibility between conserved TLs and use diverse TL haplotypes to probe the complexity of internal TL interactions.

Recent studies suggest that the primary contributor of epistasis to protein function is through pairwise residue interactions. However, higher order epistasis is complicated and can be difficult to detect (JOHNSON *et al.* 2023; METZGER *et al.* 2023). We reasoned that the Pol II TL might be an excellent system to detect higher order epistasis using evolutionary haplotypes,

notwithstanding constraints on function from the rest of the enzyme complex. The Pol II TL is flexible, required to support distinct conformational states, and functionally plastic, as mutants can both increase or decrease catalysis. Notably, known suppressor relationships between these two types of mutants highlight the complexity of residue interactions within the TL. We applied our TL deep mutational scanning system to detect higher order epistasis by comprehensive dissection of a set of evolutionarily derived TL sequences (haplotypes). We identified intra-TL interactions of evolutionarily observed substitutions (TL-internal epistasis) and dissected specific examples of complex interactions that would not be evident from simple analyses only considering single mutants or complete haplotypes. Our experiments suggest specific paths for TL evolution in the context of the complete enzyme may likely go through mild gain-of-function residues that allow additional changes to be tolerated.

RESULTS

Systematic detection of epistatic interactions within TL haplotypes. We utilized our previously developed deep mutational scanning-based phenotyping platform for Pol II mutants in *Saccharomyces cerevisiae* (QIU *et al.* 2016; DUAN *et al.* 2023) to analyze TL-internal higher-order epistasis. The analyzed TL haplotypes included 632 natural TL variants from bacterial and archaeal multi-subunit RNA polymerases (msRNAPs), and eukaryotic Pol I, Pol II and Pol III (**Fig. 1B-C**). An additional 1987 TL alleles were included, representing all possible intermediate substitution combinations for seven selected natural Pol II TL variants (**Fig. 1D**). The seven TL variants were selected because they contain specific amino acids which exhibit phenotypes, either GOF or LOF, when introduced individually in yeast Pol II. The functional consequences of these haplotypes were measured by a set of growth phenotypes that are predictive of biochemical functions (see **Methods**)(KAPLAN *et al.* 2012; QIU *et al.* 2016; QIU AND KAPLAN 2019; DUAN *et al.* 2023). The low coefficient of variation values observed in all libraries indicates high reproducibility for our measurements (**Fig. S1A**). Our system allows us to profile these haplotypes and assess epistasis among multiple mutations in a highly parallel fashion.

To detect epistasis, we first fitted a log additive model for the fitness scores of individual mutations, based on the assumption that se mutations acting independently will have log additive effects on fitness(HILL *et al.* 2008; MANI *et al.* 2008; PHILLIPS 2008; LIN *et al.* 2022; DUAN *et al.* 2023). We then calculated deviations from the expected fitness scores by comparing the observed fitness of haplotypes to these expectations (**Fig. S1B**). Any deviation from the log additive model is evidence for residue interactions (epistasis). Deviation from expectation could be in the form of mutual suppression (double mutant more fit than either single mutant), basic epistasis (double mutant no worse than one of the single mutants), or synthetic sickness (greater than log additive defects in the double mutant). The deviation values, termed “deviation scores”, were calculated to detect intra-TL genetic interactions within haplotypes (see **Methods**).

Deviation scores were calculated in two ways. First, we determined a “primary deviation” score to represent total epistasis within a haplotype. This score quantifies the deviation between the observed fitness of the haplotype to its expected fitness, which is calculated by summing the fitness scores of the individual mutants involved (**Fig. 1E and Fig. S1B**). Second, to determine which residues the epistasis emerged from, we separated the haplotypes into combinations of single substitutions and the compound mutants formed by the remaining substitutions. We therefore calculated a secondary deviation score. This score is determined by comparing the

161 observed fitness score of the haplotype to the sum of two components: the fitness score of a
162 single substitution and the fitness score of the compound formed by the remaining substitutions
163 (**Fig. 1F and Fig. S1B**). The magnitude of the secondary deviation score indicates the
164 magnitude of epistatic effects for specific substitutions when they are introduced to the
165 compound mutant. Moreover, analyzing the secondary deviation scores of a specific substitution
166 across various compound mutants (backgrounds) enables us to assess the breadth of its
167 epistatic effects, which may reveal its potential to impact TL evolution.

168 **Drivers of incompatibility for TL variants placed in the yeast Pol II context**. We
169 investigated the widespread incompatibility of TL haplotypes from various msRNAPs when
170 introduced into yeast Pol II (VIKTOROVSKAYA *et al.* 2013; QIU *et al.* 2016; DUAN *et al.* 2023). To
171 probe the incompatibility in detail, we grouped haplotypes based on their evolutionary source
172 (bacteria, archaea and eukaryotic Pol I, Pol II and Pol III). We then illustrate the fitness and
173 deviation scores in heatmaps, including the fitness of all constituent single substitutions as
174 measured in yeast Pol II (QIU *et al.* 2016; DUAN *et al.* 2023), the expected fitness of the
175 haplotypes calculated using the log additive model, the observed fitness of the haplotypes
176 measured from our deep mutational scanning, and the primary deviation score derived from
177 comparing of the observed to the expected fitness (**Fig. 2A-E**). We found that the incompatibility
178 of bacterial TLs in yeast could be explained by three substitutions that are individually lethal in
179 yeast (**Fig. 2A**). In contrast, only about half of the archaeal TLs had lethality that could be
180 explained by individually lethal substitutions. The other half appeared to be lethal due to the
181 straightforward additivity of single mutant fitness, although a subset exhibited negative epistasis
182 among the constituent substitutions (**Fig. 2B**). Eukaryotic Pol I, Pol III and Pol II haplotypes
183 exhibited fewer individually lethal single substitutions than those in bacteria and archaea.
184 However, they displayed more instances of both positive and negative intra-TL interactions (**Fig.
185 2C-G**), likely reflecting the closer evolutionary distance of these eukaryotic Pols to yeast Pol II.
186 Interestingly, a few single substitutions from other Pol II TL haplotypes caused lethality when
187 introduced into yeast Pol II context (**Fig. 2D**). We examined whether the fitness of Pol II
188 haplotypes correlates with the evolutionary distance between the genes where the TL
189 haplotypes originate and *RPB1*, where the WT TL is derived. However, we did not see a
190 significant correlation (**Fig. S2**). This could be because the TL haplotypes we picked were
191 chosen based on the diversity of single substitutions, rather than an unbiased selection across
192 evolutionary distances from *S. cerevisiae RPB1*. Therefore, we have some selection bias in our
193 haplotypes. In summary, our analyses indicate that, despite the high conservation across Pol II
194 enzymes, specific and important functional constraints have evolved among close homologs,
195 emphasizing the significance of epistasis between the TL and its Pol II context.

196 We then asked if functional coupling of residue identities within the TL across evolution might
197 correlate with positive interactions (**Fig S3A-C**). This analysis tests the hypothesis that specific
198 residues working together might be reflected by their coappearance in the TL, and if it might be
199 observable independently from their coevolved greater enzymatic contexts. Statistical coupling
200 analysis, which uses statistical inference to identify functional interactions by analyzing residue
201 identities that correlate across evolution, served as our method (RUSS *et al.* 2005; SOCOLICH *et
202 al.* 2005). Using a multiple sequence alignment of 362 eukaryotic TL sequences (natural TL
203 variants), We identified 11 residues that exhibited coupling within the TL domain (**Fig. S3A**).

204 To further explore the role of TL-internal statistical coupling in its function, particularly when
205 removed from their natural context, we designed two libraries as previously described (RUSS *et*

206 *al.* 2005; SOCOLICH *et al.* 2005). The first library consisted of scrambled haplotypes that
207 preserved TL-internal residue couplings and conservation as derived from natural TL variants
208 ("Monte Carlo" scrambling library) (**Fig. S3C**). The second library maintained only conservation
209 but not any TL-internal residue coupling ("Random scramble" library) (See **Methods**) (**Fig.**
210 **S3B**). Both libraries satisfy the design parameters as indicated by residue coupling heatmaps
211 (**Fig S3A-C**). If TL-internal coupling plays a significant role in supporting TL function, we would
212 predict that haplotypes in the Monte Carlo scramble library to exhibit higher fitness on average
213 than those in Random scramble library. However, the observed difference in fitness distributions
214 between the two libraries was subtle and statistically insignificant (P-value = 0.3013). This result
215 suggests that without the epistasis between TL alleles and their coevolved natural contexts, the
216 TL-internal epistasis is weak or undetectable.

217 **Epistasis within TL haplotypes can be attributed to specific residues.** We next determined
218 the residues from which epistatic effects in TL haplotypes emerge. We selected seven Pol II TL
219 variants, each containing 7~9 substitutions relative to the *S. cerevisiae* Pol II TL, based on their
220 diversity. We constructed 2169 combinations of all substitutions from the seven variants. Some
221 of the substitutions are shared between haplotypes, leading to repeated combinations. We kept
222 all unique haplotypes (n=1987) to ensure an equal initial allele frequency for all combinations.
223 These seven variants exhibited varying degrees of compatibility, as determined by their fitness
224 when replacing the yeast Pol II TL (**Fig. 3A-H)**. Four out of seven TL variants were incompatible
225 in the yeast Pol II context for distinct reasons. The TL variant from *G. luxurians* was lethal,
226 presumably because it encodes G1088S, which causes lethality on its own and was similarly
227 deleterious in all intermediate genotypes (**Fig. 3A, C**). In contrast, the lethalities of TL variants
228 from *B. anathema* and *R. solani* could not be explained by any individual lethal substitution.
229 They were predicted to be viable by the summation of the fitness scores of individual
230 substitutions. This suggests that the observed lethality in these two haplotypes resulted from
231 negative interactions among residues, indicating lethality beyond simple additivity (**Fig. 3A, G,**
232 **H**). The *S. rosetta* TL, however, was both expected and observed to be lethal, suggesting that
233 residue additivity causes lethality (**Fig. 3A).** Yet, it's worth noting that some intermediate
234 combinations of *S. rosetta* exhibited fitness in the lethal range **(Fig. 3F**) but were worse than
235 predicted from the log additive model, suggesting negative interactions. Interestingly, the other
236 three variants, where all individual substitutions were viable and combinations between them
237 were predicted to be viable based on the log additive model, some intermediate substitution
238 combinations fell into the severely sick or lethal range (**Fig. 3B, D, E and S4**). This implies
239 negative interactions among the substitutions. However, the lethality of these intermediate
240 genotypes was suppressed by additional substitutions, resulting in the complete, viable
241 haplotypes and indicating positive interactions (**Fig. 3B, D, E**). The fluctuations of the fitness
242 with various residue combinations suggests complexity and the potential for higher order
243 epistasis within these TL haplotypes.

244 To identify which specific residues contributed to the observed epistasis, we assessed
245 deviations from expected fitness when adding each substitution to intermediate combinations
246 derived from the original haplotypes. This analysis enabled comparisons of mutant effects
247 across multiple related backgrounds (**Fig. 1D, F and Fig. S1**). We then visualized the fitness
248 and epistatic effects of each substitution using epistasis heatmaps (**Fig. 4 and S5**). For
249 example, the *E. invadens IP1* TL haplotype exhibited better fitness than predicted by the log
250 additive model (**Fig. 4A**), suggesting positive interaction within the eight substitutions in the
251 haplotype. Among these substitutions, two have opposing biochemical phenotypes determined

252 from library screening of single mutants: the LOF V1089T and the GOF S1096E. Notably, these
253 two substitutions also displayed the lowest growth fitnesses among the eight *E. invadens IP1* TL
254 substitutions (**Fig. 4A-B**). The characteristics of these alleles suggest they are likely candidates
255 for strong epistatic effects. In support of this, S1096E consistently showed positive secondary
256 deviation scores in most intermediate combinations, suggesting its broad effects. Conversely,
257 V1089T primarily showed positive effects in combinations that contained S1096E (**Fig. 4B**),
258 suggesting that V1089T's positive effect is dependent on the presence of S1096E. This
259 dependency is likely due to a suppression effect arising from the combination of GOF and LOF
260 substitutions. Interestingly, S1091E, which lacks strong growth fitness defects and obvious
261 phenotypes as a single substitution, showed strong positive or negative epistatic effects in most
262 backgrounds (**Fig. 4B**). These results suggest that these three substitutions are key drivers of
263 intra-TL epistasis within *E. invadens IP1* TL haplotype.

264 To visualize these effects, we quantified how individual substitutions influence epistasis within
265 the haplotype. This was done by analyzing correlations between the primary deviation score,
266 which reflects the overall epistasis, and the secondary deviation scores, which detail the specific
267 epistatic effects of each substitution on different haplotype backgrounds. Substitutions
268 demonstrating strong correlation (higher linear regression R^2) are identified as the main drivers
269 of epistatic effects observed in the entire haplotype. In contrast, substitutions with low
270 correlation (smaller R^2) are considered to have limited or negligible contributions. To illustrate
271 this concept, we created a simplified simulation (**Fig. S5**). We constructed a TL haplotype
272 comprising five substitutions: a, b, c, d, and e. In this scenario, the single mutant "a" is GOF, "b"
273 and "c" are LOF, whereas "d" and "e" have no effects. We set the suppression interactions in
274 GOF+ LOF combinations (a/b and a/c), and synthetic sick interactions in the LOF+ LOF
275 combination b/c (**Fig. S5A**). We calculated both primary and secondary deviation scores for the
276 haplotype and all intermediate combinations. Notably, the GOF mutant "a" exhibited positive
277 secondary deviation scores in most intermediates (**Fig. S5B**). The secondary deviation scores
278 of three single mutants with phenotypes showed strong correlation (R^2) with the primary
279 deviation scores (**Fig. S5C**), showing that they are the key contributors to the observed epistatic
280 interactions within the haplotype. Further comparisons between the secondary deviation scores
281 of "a" versus "b" and "c" revealed positive secondary deviation scores of "b" and "c" in most
282 cases when "a" is present (**Fig. S5D**), suggesting potential suppression of "a" by "b" and "c".
283 Similarly, the secondary deviation scores of "a" are consistently positive with changes in "b"
284 (**Fig. S5E**) and "c" (**Fig. S5F**), indicating "a" suppresses "b" and "c". These observations
285 confirmed the mutual suppression in GOF and LOF combinations. Conversely, LOF
286 substitutions "b" and "c" showed correlated secondary deviation scores, showing their synthetic
287 sick interactions. These results demonstrate the behaviors that might be apparent for mutant
288 types in this form of analysis.

289 To detect the key contributors to epistatic interactions within the *E. invadens IP1* TL haplotype,
290 we determined correlations between primary and secondary deviation scores. Consistent with
291 the epistasis landscape (**Fig. 4B**), the secondary deviation scores of S1096E, V1089T, and
292 S1091E have strong correlations ($R^2 > 0.5$) with the primary deviation score (**Fig. 5A**),
293 suggesting their substantial contributions to epistasis within the haplotype. In all seven selected
294 TL variants, one to three substitutions were identified that notably affect haplotype epistasis (**Fig
295 4B, 5A, and Fig. S6-S7**), suggesting that epistasis within haplotypes is attributable to specific
296 subsets of substitutions.

297 **The epistasis within TL haplotypes can reflect intricate residue interactions**. We dissected
298 the interactions formed by the three substitutions S1096E, V1089T, and S1091E in the *E.*
299 *invadens IP1* TL haplotype, revealing an intricate, higher-order epistasis network (**Fig. 5A-G**).
300 First, we confirmed the mutual suppression between the GOF S1096E and the LOF V1089T.
301 S1096E consistently showed positive epistatic effects in haplotypes containing V1089T **(Fig.**
302 **5B**). V1089T exhibited a smaller but similar positive effect on haplotypes containing S1096E
303 (**Fig. 5C**), showing mutual suppression between them. These observations are consistent with
304 the predicted suppression between GOF and LOF mutants, as illustrated by the positive values
305 for their combinations shown in **Fig. 4B**. Additionally, we observed negative interactions
306 involving S1091E when combined with F1086H/V1089T/K1093T, in the absence of S1096E.
307 This was indicated by low secondary deviation scores for S1091E when S1096E was included
308 (**Fig. 5C**). However, S1096E exhibited consistent high scores with S1091E included (**Fig. 5D**).
309 These observations are interpreted as S1096E being epistatic to S1091E. We further identified
310 negative interactions in six intermediate combinations containing S1091E, as suggested by their
311 fitness in the ultra-sick or lethal range beyond what the log additive model predicts (**Fig. 5E**).
312 Strikingly, F1086H, V1089T, K1093T were present in all these combinations, pointing to
313 negative synergistic interaction (synthetic sickness or lethality) between the four substitutions.
314 Conversely, S1096E was absent in all these combinations (**Fig. 5E**), implying that its presence
315 suppresses the negative interaction. This suppression was further supported when the inclusion
316 of S1096E in these combinations resulted their fitness levels improved out of the sick/lethal
317 range (fitness > -5), as observed both in our high throughput system (**Fig. 5F**) and by patch
318 assay (**Fig. S8A**). We summarize all the observed interactions in **Fig. 5G**, representing the
319 complicated higher-order epistasis network.

320 We also analyzed the epistasis networks formed by substitutions inthe *P. persalinus (Ciliate)* TL
321 haplotype and identified two higher-order epistasis networks. The complexity of these networks
322 arises from the intricate layers of substitution interactions. Notably, the complex interactions
323 among these substitutions were not immediately apparent when examining the entire haplotype,
324 as the expected and observed fitnesses of the complete haplotype were similar (**Fig. 6 and Fig.**
325 **S9-S10**). First, the haplotype contains nine substitutions, each showing no or only slight growth
326 defects as single substitutions. The observed fitness of the haplotype was very similar to the
327 expected fitness calculated from the additive of all individual substitutions' fitnesses, resulting in
328 a primary deviation score close to zero. Second, when dissecting potential interactions in
329 substitution combinations, we noticed distinct behaviors in two substitutions, the predicted GOF
330 A1076T and LOF V1089S. We anticipated a suppression interaction between them and
331 predicted that they would be drivers of epistatic interactions within intermediate combinations.
332 Consistently, we observed suppression when A1076T and V1089S were combined (**Fig. S9**),
333 and correlations between the secondary and primary deviation scores suggest that these two
334 substitutions strongly affect the epistasis in the haplotypes (**Fig. 6B**). Third, we identified two
335 intermediate combinations, each with five substitutions, that exhibited the lowest primary and
336 secondary deviation scores (the labeled **I** and **II in Fig. 6B**). These low scores imply negative
337 interactions such as synthetic sickness or lethality.

338 The combination I, A1076T/A1090S/S1091D/S1096L/I1104L, showed a negative primary
339 deviation score (observed fitness < expected fitness) (**Fig. 6C**), illustrating synthetic sickness
340 among the five substitutions. The secondary deviation scores of five constituent substitutions
341 were all negative (**Fig. 6C**), implying that each addition worsened the fitness. Conversely, the
342 remaining four substitutions, V1089S, K1092R, K1093N, and K1102Q, all showed positive

343 secondary deviation scores when incorporated into the combination. This suggests each one
344 could individually suppress the synthetic sick combination (**Fig. 6C**). We validated the
345 suppression by V1089S to the combination by spot assay and doubling time (**Fig. S8B-C**). The
346 consistency indicates the interactions we observed in the high throughput experiment are
347 reliable. The observed interaction network is shown in **Fig. 6D**.

348 In contrast, combination II (A1076T/A1090S/S1091D/K1092R/K1093N) exhibited sign epistasis,
349 where the GOF sign of A1076T appeared to change to LOF in the presence of the other four
350 substitutions simultaneously. In detail, the combination II has a negative primary deviation
351 score, representing negative interaction among five substitutions (**Fig. 6E**). Surprisingly, the
352 negative interaction appeared only when the four substitutions, A1090S, S1091D, K1092R, and
353 K1093N were present simultaneously with A1076T (**Fig. S10A**). Notably, no obvious
354 interactions occur among these four substitutions alone (**Fig. S9**), suggesting the interaction is
355 between A1076T and the combination of the four substitutions
356 (A1090S/S1091D/K1092R/K1093N). We further inferred a change in A1076T from GOF to LOF,
357 particularly due to the observed lethality when LOF V1089S was incorporated into the
358 combination. Notably, while A1076T generally suppresses V1089S in almost all synthetic sick or
359 lethal backgrounds involving V1089S and the individual or combinations of A1090S, S1091D,
360 K1092R, and K1093N, it exacerbates the growth defect when combined with
361 V1089S/A1090S/S1091D/K1092R/K1093N. This outcome aligns with the expected lethality
362 when the same class substitutions are combined (LOF V1089S and the LOF A1076T) (**Fig.
363 S10B-C**). These observations suggest that the combination A1090S/S1091D/K1092R/K1093N
364 converts A1076T from GOF to LOF. Further supporting this, when S1096L, K1102Q, and
365 I1104L are individually included in the combination A1076T/A1090S/S1091D/K1092R/K1093N,
366 each one suppresses the combination, as evidenced by their positive secondary deviation
367 scores (**Fig. 6E**). The weak suppression between I1104L and the combination was also
368 confirmed by comparison in doubling time (**Fig. S8C**). The suppression interactions imply that
369 each one of them can individually revert the sign epistasis within
370 A1076T/A1090S/S1091D/K1092R/K1093N. As a result, A1076T is back to GOF, and LOF
371 V1089S becomes suppressible by GOF A1076T (**Fig. 6F**). In summary, these intricate
372 interaction networks observed in the *P. persalinus (Ciliate)* TL haplotype (**Fig. 6E-F**) emphasize
373 the complexity of higher-order epistasis, revealing layers of interactions beneath the surface.

374 **Distinct categories of residue epistasis patterns**. To comprehensively compare the
375 magnitude and consistency of epistatic effects of TL substitutions across different genetic
376 backgrounds, we determined the distributions of secondary deviation scores for each
377 substitution. Substitutions with strong epistatic effect (**Fig. 4 and S6**) and primary/secondary
378 score correlations (**Fig. 5A, Fig. 6B, and Fig. S7**) exhibited wide distributions of secondary
379 deviation scores. Interestingly, while most of these impactful substitutions have classifiable
380 phenotypes as single substitutions (GOF or LOF) (**Fig. S11A-F**), others without obvious
381 phenotypes, such as S1091E (**Fig. S11A**), K1093N (**Fig. S11E-F**), A1076G and N1082K (**Fig.
382 S11G**), still showed wide ranges of epistatic impacts. Notably, some substitutions, like A1076T,
383 were present in more than one TL haplotype background (**Fig. S11C-F**). To evaluate the overall
384 epistatic effects of these substitutions in all tested backgrounds, we displayed the density plots
385 of their secondary deviation scores across all non-repetitive haplotypes (**Fig. S12**) and
386 calculated the maximum likelihood estimate (σ^2) to quantify the distribution of secondary
387 deviation scores for each substitution (PARK *et al.* 2022) (**Fig. 7A**). We found that 62.5% of
388 substitutions exhibited mild epistatic effects ($\sigma^2 < 3$) and, 25% showed medium effect ($3 \leq \sigma 2 \leq$

389 5). A small portion, 12.5% of substitutions, had strong epistatic effects ($\sigma^2 > 5$). The epistatic
390 effects of substitutions did not correlate with their fitness as single substitutions (**Fig. S13A**).
391 Moreover, if the substitution has no or minor epistatic effect in backgrounds to which it is
392 introduced, its secondary deviation scores are expected to follow normal distribution (PARK *et al.*
393 2022). However, approximately 80% of TL substitutions did not have normally distributed
394 secondary deviation scores (**Fig. S13B**), illustrating that most TL substitutions had epistatic
395 effects when introduced into some if not all genetic backgrounds. To investigate whether the
396 epistatic effects of substitutions consistently remained positive (or negative) across various
397 genetic backgrounds, we calculated the median of secondary deviation scores for each
398 substitution and plotted them against the corresponding σ^2 values. Substitutions with strong
399 epistatic effects (σ^2) exhibited higher positive (or negative) median values (**Fig. 7B**), implying
400 that robust epistatic effects were consistently positive or negative across various genetic
401 backgrounds. We further compared the epistatic effects of substitutions in three categories (**Fig.
402 7C**). Substitutions with mild epistatic effects had little impact on the fitness of haplotypes when
403 introduced. Substitutions with medium epistatic effects, like A1076T and K1093N, could either
404 enhance or reduce haplotype fitness. In contrast, substitutions with strong epistatic effects, such
405 as S1096E and R1100C, were epistatic to backgrounds in which they were observed, consistent
406 with their requirement for tolerance of specific substitutions in those backgrounds.

407 **DISCUSSION**

408 RNA polymerase TL function and evolution are impacted by extensive residue interactions
409 within and around it (KAPLAN *et al.* 2012; DUAN *et al.* 2023). The TL shows remarkable
410 conservation, consistent with its essential role in executing transcription mechanisms in all
411 msRNAPs (CRAMER 2002; WERNER AND GROHMANN 2011; BELOGUROV AND ARTSIMOVITCH
412 2019; MAZUMDER *et al.* 2020; KULDELL AND KAPLAN 2024). Our observation of widespread TL
413 incompatibility in the *S. cerevisiae* Pol II context suggested that epistasis external to the TL is
414 the major source of epistasis affecting TL function (DUAN *et al.* 2023) (**Fig. S3**). However, here
415 we observed TL-internal epistatic interactions and residue coupling, although TL-internal
416 coupling did not significantly maintain TL function when the interaction between TL and its
417 broader evolutionary context was disrupted. The analyses in our recent work (DUAN *et al.* 2023)
418 and here indicate that interactions formed by TL residues are integrated into the broader residue
419 epistasis network within the whole enzyme (**Fig. 2**). These results align with other studies
420 showing that the same mutation led to different phenotypes when introduced into homologous
421 proteins (KONDRASHOV *et al.* 2002; LUNZER *et al.* 2010; NATARAJAN *et al.* 2013; VIKTOROVSKAYA
422 *et al.* 2013; DOUD *et al.* 2015; STARR AND THORNTON 2016; HADDOX *et al.* 2018; PARK *et al.*
423 2022), highlighting the divergent nature of epistasis networks even in highly conserved proteins
424 like msRNAPs.

425 Our experiments here provide case studies for examples of complex interactions during
426 evolutionary divergence. Epistasis networks of homologs diverge through accumulated
427 substitutions. Understanding how substitutions alter existing epistasis and shape the effects of
428 future substitutions is critical for elucidating mechanisms underlying protein functional
429 divergence and evolution (STARR AND THORNTON 2016; JOHNSON *et al.* 2023; XIE *et al.* 2023).
430 Using seven selected Pol II TL variants, we comprehensively determined the higher-order
431 epistatic interactions created by these substitutions. For example, S1096E exhibited strong
432 suppression on all synthetic sick/lethal combinations in the *E. invadens IP1* TL haplotype (**Fig. 5
433 and S8**), suggesting a potential evolutionary pathway for TL where the 1096E substitution
434 occurs prior to additional substitutions that lead to synthetic sickness or lethality. A caveat to this

435 interpretation is that additional substitutions outside the TL might reshape epistasis across the
436 entire TL. Additionally, A1076T, a substitution that consistently showed positive epistatic effects
437 when introduced into different genetic backgrounds (**Fig. 7C**), was also subject to sign epistasis
438 in certain backgrounds. Here, we would propose that additional substitutions preventing this
439 sign epistasis might precede the appearance of combinations that would otherwise incur a
440 fitness defect with A1076T (**Fig. 6E-F**). The sign epistasis involving A1076T exemplifies the
441 intricate layers of substitution interactions, where emerging substitutions modify pre-existing
442 interactions, ultimately influencing the fate of future mutations and the trajectory of protein
443 evolution.

444 We further inquired whether individual substitutions could alter pre-existing epistasis networks in
445 the protein background they were introduced into, and to what extent. To address this, we
446 analyzed the strength and consistency of the epistatic effects of substitutions across diverse
447 genetic backgrounds. TL substitutions can be categorized into three groups based on their
448 epistatic effects. Approximately 37.5% of TL substitutions consistently demonstrated medium to
449 strong, stable epistatic effects, either positive or negative (**Fig. 7A-B**), reflecting their important
450 role in reshaping the interactions among fixed historical substitutions and influencing the
451 phenotypes of upcoming mutations. Substitutions that consistently exhibit positive epistatic
452 effects, such as A1076T and S1096E (**Fig. 7C**), are referred to as "permissive substitutions"
453 (STARR AND THORNTON 2016). They have the potential to make certain mutations accessible
454 that would otherwise remain inaccessible. An obvious path for evolutionary divergence in
455 msRNAPs would be the incorporation of substitutions with mild effects on fitness but with
456 biochemical properties of increased catalytic activity. These GOF alleles would have properties
457 of suppression of LOF alleles that might otherwise be selected against. Conversely,
458 substitutions with a consistent negative effect, like K1093N and R1100C, may act as "restrictive
459 substitutions", limiting the accessibility of some mutations (STARR AND THORNTON 2016). A
460 limitation of our analyses is that it tested a limited number of backgrounds. In the future, our
461 platform has the capability to determine if the case studies presented here are rarer or the norm
462 in the TL. In summary, our analyses provide a framework for understanding complicated
463 epistatic interactions of substitutions and examples of how fitness landscapes of mutants are
464 changed due to epistasis.

465 **METHODS**

466 **Experimental data**

467 Experimental data was collected as described in Duan et al (DUAN *et al.* 2023). Briefly, we
468 synthesized TL mutant libraries including 632 natural TL variants from 182 bacterial, 116
469 archaeal, and 333 eukaryotic RNA polymerases (Pol I TLs n = 144, Pol II TLs n = 94, Pol III TLs
470 n = 95) to detect their compatibility in *S. cerevisiae* background. Additionally, to identify internal
471 interactions within TL haplotypes, we selected seven Pol II TL natural variants from eukaryotic
472 Pol II (names of the selected species are as described in **Fig. 3B-H**), and synthesized 1987 TL
473 haplotypes encompassing every possible substitution combination among the seven selected
474 Pol II TL haplotypes. Furthermore, we designed and synthesized 724 Pol II TL haplotypes
475 specifically for coupling analysis. Lastly, 620 TL single mutants serving as control to determine
476 residue interactions. Approximate 15% wild-type *S. cerevisiae* Pol II TL allele of total variants
477 was incorporated into each TL library for accurate quantification. All TL alleles were amplified
478 and transformed into yeast strain CKY283 along with modified *RPO21/RPB1*-encoding plasmid
479 to allow construction of complete *rpb1* TL mutants within yeast through gap repair. After
480 transformation, Leu+ colonies were collected, and re-plated into subsequent selection plates
481 (SC-Leu+20mg/L Mg, SC-Leu+15mM Mn, YPRaff, YPRaffGal, SC-Lys, and SC-Leu+3% Form).

Growth defects and phenotypes of mutants were assessed through amplicon sequencing with Illumina Next-seq (150nt reads). We carefully constructed amplicon sequencing libraries. We performed emulsion PCR on the TL region to amplify the mutants in the libraries while minimize template switching. Additionally, PCR was done with optimized cycles to preserve original allele frequencies. Subsequently, we employed dual indices for multiplexing samples.

Data cleaning and normalization

Each TL variant library was constructed and subject to screening in three biological replicates. After screening, TL regions of mutants in the variant libraries were amplified and sequenced. The read counts of mutants were estimated by a codon-based alignment algorithm (SING-HOI SZE 2018), and the median of these counts from the three replicates was used for calculating growth defects in subsequent analysis. Growth defects of mutants were represented with a fitness metric. Fitness is determined by comparing the shifts in allele frequency of a mutant under selective conditions compared to control conditions, with these shifts further compared against changes observed in the WT. The log of the comparison is defined as a fitness. The formula used for this calculation is detailed below.

Fitness score (mutant) = $\log [f^{\text{mutant, selected}} / f^{\text{mutant, unselected}}] - \log [f^{\text{WT, selected}} / f^{\text{WT, unselected}}]$ (f represents allele frequency of a certain variant in this formula).

To enable direct comparisons between libraries, we applied min-max normalization to standardize median growth fitness across all variants. Residue with fitness equal or smaller to -6.5 was categorized within the severe sick and lethality range, and their fitness are normalized to the lethal threshold of -6.5, ensuring consistency in the severity classification.

Determination of functional interactions

Functional interactions were represented by genetic interactions, calculated using the log additive model(**Fig. S1B**). This model assumes individual mutations act independent, and their effects are multiplied in the double/multiple mutants. In our case, the fitness scores are expressed in logarithmic form, so these effects become additive.

Primary deviation score of a putative haplotype (abc) = Fitness (abc) – [Fitness (a) + Fitness (b) + Fitness (c)].

We further selected seven Pol II TL alleles and constructed all intermediate substitution combinations. For example, the putative TL haplotype has three different residues compared with wild-type *S. cerevisiae* Pol II TL allele a, b and c, we constructed all combinations of substitutions, which are a, b, c, ab, ac, bc, and abc. And we can calculate the secondary deviation scores for each substitution a, b and c. The secondary deviation score of a are calculated from all haplotypes containing a: Secondary deviation score of a_1 = Fitness (ab) – Fitness (b). Secondary deviation score of a_2 = Fitness (ac) – Fitness (c). Secondary deviation score of a_3= Fitness (abc) – Fitness (bc).

Primary and secondary deviation scores cannot be determined if the expected and observed fitness are both in the sick/lethal range (both fitness < -6.5). Haplotypes with expected fitness < -6.5 can be separated into two different situations. First, when all constituent substitutions are viable, but the sum of the fitness is lower than -6.5. This would be consistent with lethality due to additivity and indicated with a dark gray block in the deviation score heatmaps. Second, when some of the constituent substitutions or combinations are in lethal range, this lethality is

reasoned to derived from the haplotype containing at least one individually lethal substitution and indicated with a black block in the deviation heatmap.

Functional interactions are determined from deviation scores. Positive interaction (suppression): deviation score > 1. Additive (No interaction): -1 ⩽ deviation score ⩽ 1. Negative interaction (synthetic sickness/lethality): deviation score < -1.

Maximum likelihood estimate (σ^2) of a certain substitution is calculated to represent its overall epistatic effect (PARK *et al.* 2022). For a substitution with n non-repetitive secondary deviation scores, its maximum likelihood estimate: $\sigma^2 = \frac{\sum_n (Secondary\ deviation\ score\ of\ a\ substitution)^2}{n}$

Coupling analysis

Coupling analysis was done as described in Russ et al (RUSS *et al.* 2005) and Socolich et al (SOCOLICH *et al.* 2005) using a multiple sequence alignment (MSA) of Pol II TL sequences. Briefly, three independent TL haplotypes libraries were constructed to study intra-TL co-evolutionary residues. (a). Natural variants library, which consists of 362 selected natural eukaryotic Pol I, II, and III TL variants. To detect potential coupled residues, these TL variants were aligned using multiple sequence alignment, followed by coupling analysis. (**Fig. S3A**). (b). Random scrambling library, where amino acids in the same position of the MSA from (a) were randomly swapped. This swapping does not disturb sequence conservation, because the composition of different amino acids in the position remains unchanged but disrupts residue coupling among different residues. Coupling analysis was done for the random scrambled MSA to confirm disrupted residue coupling (**Fig. S3B**). (c). Monte Carlo scrambling library, where the amino acids in the same position were swapped and then assessed by the Monte Carlo algorithm. If the swapping perturbs residue coupling, we withdraw the swap; if not, we keep the swap. By doing this, the Monte Carlo scrambling library retains both sequence conservation and residue coupling information (**Fig. S3C**). The swapping in both cases breaks the epistasis between TL residues and the Pol II context. TL haplotypes were synthesized based on three types of MSA and then screened for mutant phenotypes through phenotypic system (QIU *et al.* 2016; QIU AND KAPLAN 2019; DUAN *et al.* 2023).

Doubling time measurement

TL variants were tested in four biological replicates, each with three or four biological replicates. Overnight cultures of all variants were diluted to an OD of 0.005 in 200 µL YPD and grown at 30°C, with OD measurements taken every 30 minutes for 48 hours. The experiment was done using a Tecan Spark Microplate Reader. R package Growthcurver (version 0.3.1) was used in analysis for obtaining doubling time (SPROUFFSKE AND WAGNER 2016).

DATA AVAILABILITY

Raw sequencing data has been deposited on the NCBI SRA (Sequence Read Archive) database under BioProject PRJNA948661. Processed mutant count, fitness and processing codes are available through GitHub (https://github.com/Kaplan-Lab-Pitt/TLs_Screening.git). Strains and plasmids will be provided upon request.

FUNDING

We acknowledge funding from NIH R01GM097260 for initiation of this project and NIH R35GM144116 for this work. This research was supported in part by the University of Pittsburgh Center for Research Computing RRID:SCR_022735 through the resources provided.

Specifically, this work used the HTC cluster, which is supported by NIH award number S10OD028483.

AUTHOR CONTRIBUTION

BD performed sequencing library construction, data analysis, and made figures, drafted and revised the manuscript. CQ designed the mutant libraries, performed screening experiments and statistical coupling analysis, and contributed to revise the manuscript. SZ counted the mutants from raw sequencing data. SWL contributed to experimental design and manuscript revision. CDK conceived the project, guided analyses and interpretation of data, provided funding, revised the manuscript.

ACKNOWLEDGMENTS

We thank Dr. Anne-Ruxandra Carvunis (U. Pittsburgh) for discussions and advice. We thank Zhizhen Wang and Muyao Lin from the Pitt Statistical Consulting Center for their advice on checking the reproducibility of our data.

CONFLICT OF INTEREST

The authors declare no conflict of interest.

REFERENCES

Bakerlee, C. W., A. N. Nguyen Ba, Y. Shulgina, J. I. Rojas Echenique and M. M. Desai, 2022 Idiosyncratic epistasis leads to global fitness-correlated trends. Science 376**:** 630-635.

Bank, C., R. T. Hietpas, J. D. Jensen and D. N. Bolon, 2015 A systematic survey of an intragenic epistatic landscape. Mol Biol Evol 32**:** 229-238.

Bar-Nahum, G., V. Epshtein, A. E. Ruckenstein, R. Rafikov, A. Mustaev *et al.*, 2005 A ratchet mechanism of transcription elongation and its control. Cell 120**:** 183-193.

Barnes, C. O., M. Calero, I. Malik, B. W. Graham, H. Spahr *et al.*, 2015 Crystal Structure of a Transcribing RNA Polymerase II Complex Reveals a Complete Transcription Bubble. Mol Cell 59**:** 258-269.

Belogurov, G. A., and I. Artsimovitch, 2019 The Mechanisms of Substrate Selection, Catalysis, and Translocation by the Elongating RNA Polymerase. J Mol Biol 431**:** 3975-4006.

Braberg, H., H. Jin, E. A. Moehle, Y. A. Chan, S. Wang *et al.*, 2013 From structure to systems: high-resolution, quantitative genetic analysis of RNA polymerase II. Cell 154**:** 775-788.

Cheung, A. C., and P. Cramer, 2011 Structural basis of RNA polymerase II backtracking, arrest and reactivation. Nature 471**:** 249-253.

Cramer, P., 2002 Multisubunit RNA polymerases. Curr Opin Struct Biol 12**:** 89-97.

Da, L. T., D. Wang and X. Huang, 2012 Dynamics of pyrophosphate ion release and its coupled trigger loop motion from closed to open state in RNA polymerase II. J Am Chem Soc 134**:** 2399-2406.

Dangkulwanich, M., T. Ishibashi, S. Liu, M. L. Kireeva, L. Lubkowska *et al.*, 2013 Complete dissection of transcription elongation reveals slow translocation of RNA polymerase II in a linear ratchet mechanism. Elife 2**:** e00971.

Ding, D., A. G. Green, B. Wang, T. V. Lite, E. N. Weinstein *et al.*, 2022 Co-evolution of interacting proteins through non-contacting and non-specific mutations. Nat Ecol Evol 6**:** 590-603.

Domingo, J., P. Baeza-Centurion and B. Lehner, 2019 The Causes and Consequences of Genetic Interactions (Epistasis). Annu Rev Genomics Hum Genet 20**:** 433-460.

Doud, M. B., O. Ashenberg and J. D. Bloom, 2015 Site-Specific Amino Acid Preferences Are Mostly Conserved in Two Closely Related Protein Homologs. Mol Biol Evol 32**:** 2944-2960.

Duan, B., C. Qiu, S. H. Sze and C. Kaplan, 2023 Widespread epistasis shapes RNA Polymerase II active site function and evolution. bioRxiv.

614 Fouqueau, T., M. E. Zeller, A. C. Cheung, P. Cramer and M. Thomm, 2013 The RNA
615 polymerase trigger loop functions in all three phases of the transcription cycle. Nucleic
616 Acids Res 41: 7048-7059.
617 Haddox, H. K., A. S. Dingens, S. K. Hilton, J. Overbaugh and J. D. Bloom, 2018 Mapping
618 mutational effects along the evolutionary landscape of HIV envelope. Elife 7.
619 Hill, W. G., M. E. Goddard and P. M. Visscher, 2008 Data and theory point to mainly additive
620 genetic variance for complex traits. PLoS Genet 4: e1000008.
621 Huang, X., D. Wang, D. R. Weiss, D. A. Bushnell, R. D. Kornberg *et al.*, 2010 RNA polymerase
622 II trigger loop residues stabilize and position the incoming nucleotide triphosphate in
623 transcription. Proc Natl Acad Sci U S A 107: 15745-15750.
624 Johnson, M. S., G. Reddy and M. M. Desai, 2023 Epistasis and evolution: recent advances and
625 an outlook for prediction. BMC Biol 21: 120.
626 Kaplan, C. D., 2010 The architecture of RNA polymerase fidelity. BMC Biol 8: 85.
627 Kaplan, C. D., 2013 Basic mechanisms of RNA polymerase II activity and alteration of gene
628 expression in Saccharomyces cerevisiae. Biochimica Et Biophysica Acta-Gene
629 Regulatory Mechanisms 1829: 39-54.
630 Kaplan, C. D., H. Jin, I. L. Zhang and A. Belyanin, 2012 Dissection of Pol II trigger loop function
631 and Pol II activity-dependent control of start site selection in vivo. PLoS Genet 8:
632 e1002627.
633 Kaplan, C. D., K. M. Larsson and R. D. Kornberg, 2008 The RNA polymerase II trigger loop
634 functions in substrate selection and is directly targeted by alpha-amanitin. Mol Cell 30:
635 547-556.
636 Kireeva, M. L., Y. A. Nedialkov, G. H. Cremona, Y. A. Purtov, L. Lubkowska *et al.*, 2008
637 Transient reversal of RNA polymerase II active site closing controls fidelity of
638 transcription elongation. Mol Cell 30: 557-566.
639 Kondrashov, A. S., S. Sunyaev and F. A. Kondrashov, 2002 Dobzhansky-Muller
640 incompatibilities in protein evolution. Proc Natl Acad Sci U S A 99: 14878-14883.
641 Kuldell, J. C., and C. D. Kaplan, 2024 RNA Polymerase II Activity Control of Gene Expression
642 and Involvement in Disease. Journal of Molecular Biology.
643 Kumar, S., M. Suleski, J. M. Craig, A. E. Kasprowicz, M. Sanderford *et al.*, 2022 TimeTree 5: An
644 Expanded Resource for Species Divergence Times. Molecular Biology and Evolution 39.
645 Larson, M. H., J. Zhou, C. D. Kaplan, M. Palangat, R. D. Kornberg *et al.*, 2012 Trigger loop
646 dynamics mediate the balance between the transcriptional fidelity and speed of RNA
647 polymerase II. Proc Natl Acad Sci U S A 109: 6555-6560.
648 Lin, X., Y. Liu, S. Liu, X. Zhu, L. Wu *et al.*, 2022 Nested epistasis enhancer networks for robust
649 genome regulation. Science 377: 1077-1085.
650 Liu, B., Y. Zuo and T. A. Steitz, 2016 Structures of E. coli sigmaS-transcription initiation
651 complexes provide new insights into polymerase mechanism. Proc Natl Acad Sci U S A
652 113: 4051-4056.
653 Lunzer, M., G. B. Golding and A. M. Dean, 2010 Pervasive cryptic epistasis in molecular
654 evolution. PLoS Genet 6: e1001162.
655 Malinen, A. M., M. Turtola, M. Parthiban, L. Vainonen, M. S. Johnson *et al.*, 2012 Active site
656 opening and closure control translocation of multisubunit RNA polymerase. Nucleic
657 Acids Res 40: 7442-7451.
658 Mani, R., R. P. St Onge, J. L. t. Hartman, G. Giaever and F. P. Roth, 2008 Defining genetic
659 interaction. Proc Natl Acad Sci U S A 105: 3461-3466.
660 Mazumder, A., M. Lin, A. N. Kapanidis and R. H. Ebright, 2020 Closing and opening of the RNA
661 polymerase trigger loop. Proc Natl Acad Sci U S A 117: 15642-15649.
662 Melamed, D., D. L. Young, C. E. Gamble, C. R. Miller and S. Fields, 2013 Deep mutational
663 scanning of an RRM domain of the Saccharomyces cerevisiae poly(A)-binding protein.
664 RNA 19: 1537-1551.

Metzger, B. P. H., Y. Park, T. N. Starr and J. W. Thornton, 2023 Epistasis facilitates functional evolution in an ancient transcription factor. Elife.

Mosaei, H., and N. Zenkin, 2021 Two distinct pathways of RNA polymerase backtracking determine the requirement for the Trigger Loop during RNA hydrolysis. Nucleic Acids Res 49**:** 8777-8784.

Natarajan, C., N. Inoguchi, R. E. Weber, A. Fago, H. Moriyama *et al.*, 2013 Epistasis among adaptive mutations in deer mouse hemoglobin. Science 340**:** 1324-1327.

Nayak, D., M. Voss, T. Windgassen, R. A. Mooney and R. Landick, 2013 Cys-pair reporters detect a constrained trigger loop in a paused RNA polymerase. Mol Cell 50**:** 882-893.

Olson, C. A., N. C. Wu and R. Sun, 2014 A comprehensive biophysical description of pairwise epistasis throughout an entire protein domain. Curr Biol 24**:** 2643-2651.

Palo, M. Z., J. Zhu, T. V. Mishanina and R. Landick, 2021 Conserved Trigger Loop Histidine of RNA Polymerase II Functions as a Positional Catalyst Primarily through Steric Effects. Biochemistry 60**:** 3323-3336.

Park, Y., B. P. H. Metzger and J. W. Thornton, 2022 Epistatic drift causes gradual decay of predictability in protein evolution. Science 376**:** 823-830.

Phillips, P. C., 1998 The language of gene interaction. Genetics 149**:** 1167-1171.

Phillips, P. C., 2008 Epistasis--the essential role of gene interactions in the structure and evolution of genetic systems. Nat Rev Genet 9**:** 855-867.

Pokusaeva, V. O., D. R. Usmanova, E. V. Putintseva, L. Espinar, K. S. Sarkisyan *et al.*, 2019 An experimental assay of the interactions of amino acids from orthologous sequences shaping a complex fitness landscape. PLoS Genet 15**:** e1008079.

Qiu, C., O. C. Erinne, J. M. Dave, P. Cui, H. Jin *et al.*, 2016 High-Resolution Phenotypic Landscape of the RNA Polymerase II Trigger Loop. PLoS Genet 12**:** e1006321.

Qiu, C., and C. D. Kaplan, 2019 Functional assays for transcription mechanisms in high-throughput. Methods 159-160**:** 115-123.

Reddy, G., and M. M. Desai, 2021 Global epistasis emerges from a generic model of a complex trait. Elife 10.

Russ, W. P., D. M. Lowery, P. Mishra, M. B. Yaffe and R. Ranganathan, 2005 Natural-like function in artificial WW domains. Nature 437**:** 579-583.

Seibold, S. A., B. N. Singh, C. Zhang, M. Kireeva, C. Domecq *et al.*, 2010 Conformational coupling, bridge helix dynamics and active site dehydration in catalysis by RNA polymerase. Biochim Biophys Acta 1799**:** 575-587.

Sing-Hoi Sze, C. D. K., 2018 Codon-Based Sequence Alignment for Mutation Analysis by High-Throughput Sequencing, pp. in *2018 IEEE 8th International Conference on Computational Advances in Bio and Medical Sciences (ICCABS)*.

Socolich, M., S. W. Lockless, W. P. Russ, H. Lee, K. H. Gardner *et al.*, 2005 Evolutionary information for specifying a protein fold. Nature 437**:** 512-518.

Sprouffske, K., and A. Wagner, 2016 Growthcurver: an R package for obtaining interpretable metrics from microbial growth curves. BMC Bioinformatics 17.

Starr, T. N., and J. W. Thornton, 2016 Epistasis in protein evolution. Protein Sci 25**:** 1204-1218.

Sydow, J. F., F. Brueckner, A. C. Cheung, G. E. Damsma, S. Dengl *et al.*, 2009 Structural basis of transcription: mismatch-specific fidelity mechanisms and paused RNA polymerase II with frayed RNA. Mol Cell 34**:** 710-721.

Tamura, K., G. Stecher, S. Kumar and F. U. Battistuzzi, 2021 MEGA11: Molecular Evolutionary Genetics Analysis Version 11. Molecular Biology and Evolution 38**:** 3022-3027.

Unarta, I. C., E. C. Goonetilleke, D. Wang and X. Huang, 2023 Nucleotide addition and cleavage by RNA polymerase II: Coordination of two catalytic reactions using a single active site. J Biol Chem 299**:** 102844.

Vassylyev, D. G., M. N. Vassylyeva, J. Zhang, M. Palangat, I. Artsimovitch *et al.*, 2007 Structural basis for substrate loading in bacterial RNA polymerase. Nature 448**:** 163-168.

716 Viktorovskaya, O. V., K. L. Engel, S. L. French, P. Cui, P. J. Vandeventer *et al.*, 2013 Divergent
717 contributions of conserved active site residues to transcription by eukaryotic RNA
718 polymerases I and II. Cell Rep 4**:** 974-984.
719 Wang, B., A. V. Predeus, Z. F. Burton and M. Feig, 2013 Energetic and structural details of the
720 trigger-loop closing transition in RNA polymerase II. Biophys J 105**:** 767-775.
721 Wang, D., D. A. Bushnell, X. Huang, K. D. Westover, M. Levitt *et al.*, 2009 Structural basis of
722 transcription: backtracked RNA polymerase II at 3.4 angstrom resolution. Science 324**:**
723 1203-1206.
724 Wang, D., D. A. Bushnell, K. D. Westover, C. D. Kaplan and R. D. Kornberg, 2006 Structural
725 basis of transcription: role of the trigger loop in substrate specificity and catalysis. Cell
726 127**:** 941-954.
727 Werner, F., and D. Grohmann, 2011 Evolution of multisubunit RNA polymerases in the three
728 domains of life. Nat Rev Microbiol 9**:** 85-98.
729 Windgassen, T. A., R. A. Mooney, D. Nayak, M. Palangat, J. Zhang *et al.*, 2014 Trigger-helix
730 folding pathway and SI3 mediate catalysis and hairpin-stabilized pausing by Escherichia
731 coli RNA polymerase. Nucleic Acids Res 42**:** 12707-12721.
732 Xie, X., X. Sun, Y. Wang, B. Lehner and X. Li, 2023 Dominance vs epistasis: the biophysical
733 origins and plasticity of genetic interactions within and between alleles. Nat Commun 14**:**
734 5551.
735 Xu, L., K. V. Butler, J. Chong, J. Wengel, E. T. Kool *et al.*, 2014 Dissecting the chemical
736 interactions and substrate structural signatures governing RNA polymerase II trigger
737 loop closure by synthetic nucleic acid analogues. Nucleic Acids Res 42**:** 5863-5870.
738 Yuzenkova, Y., A. Bochkareva, V. R. Tadigotla, M. Roghanian, S. Zorov *et al.*, 2010 Stepwise
739 mechanism for transcription fidelity. BMC Biol 8**:** 54.
740 Zhang, J., M. Palangat and R. Landick, 2010 Role of the RNA polymerase trigger loop in
741 catalysis and pausing. Nat Struct Mol Biol 17**:** 99-104.

742

743

744 **Figures**

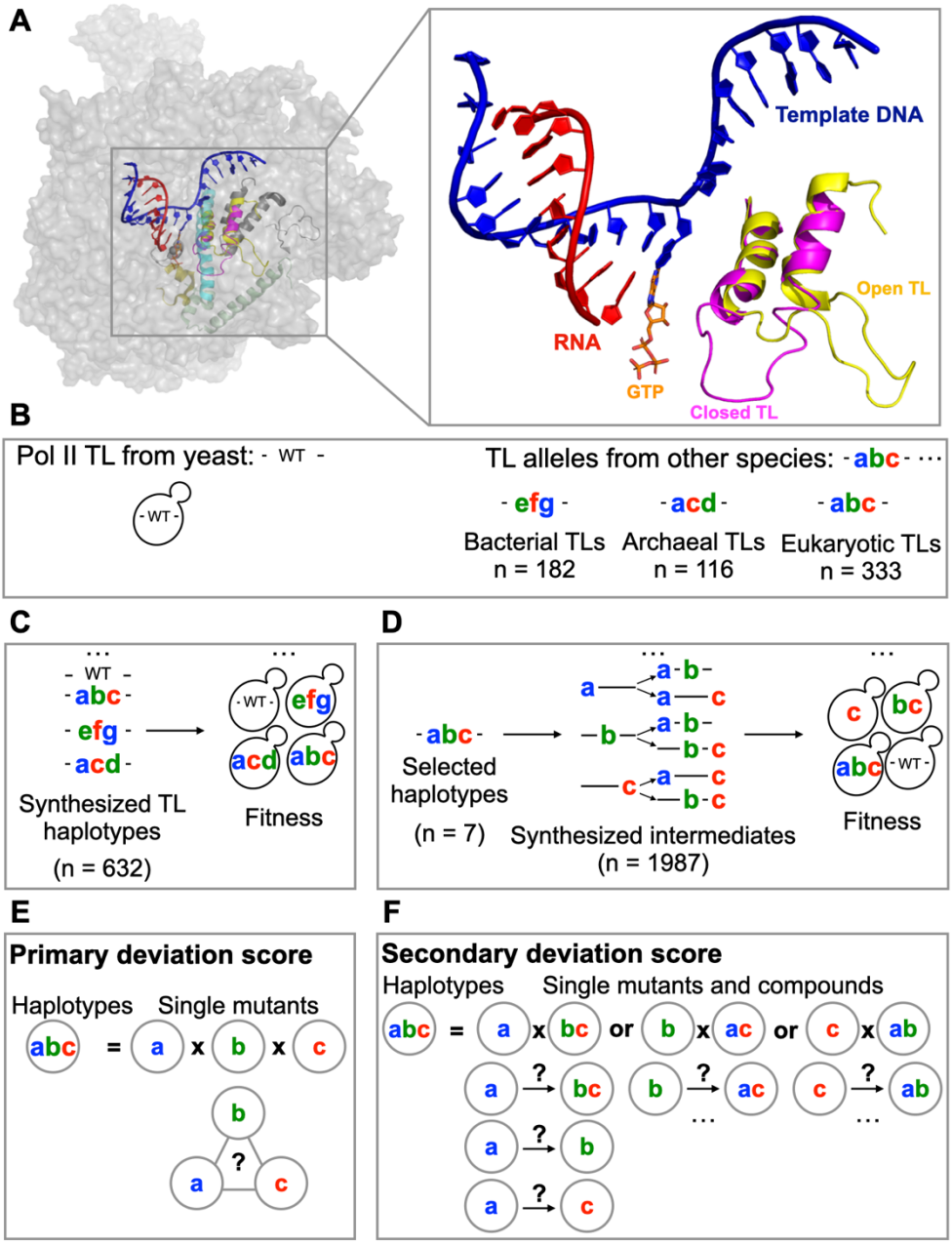

745

746

747 **Figure 1. Systematic detection of TL-internal epistasis with natural TL alleles and**
748 **intermediates. A**. The Pol II TL is the key domain balancing transcription speed and fidelity in
749 Pol II active site. Left panel: yeast Pol II structure (PDB: 5C4X). Right panel: The open, catalytic
750 disfavoring (PDB: 5C4X) (BARNES *et al.* 2015) and closed, catalytic favoring (PDB: 2E2H)
751 (WANG *et al.* 2006) conformations of TL in the active site. **B**. We selected 632 TL haplotypes
752 representing TL alleles from bacterial, archaeal and the three conserved eukaryotic msRNAPs
753 to detect TL-internal epistasis (Bacterial TLs n = 182, archaeal TLs n = 116, Pol I TLs n = 144,
754 Pol II TLs n = 94, Pol III TLs n = 95). **C**. The selected TL alleles were synthesized and

755 transformed into yeast Pol II to form chimeric Pol II enzymes. Yeast chimeric Pol II enzymes
756 were phenotyped under selective conditions to detect growth defects, which are represented by
757 fitness (see **Methods**). **D**. Seven Pol II TL alleles were selected to construct intermediate
758 haplotypes representing all possible combinations of substitutions of the seven selected alleles.
759 The intermediates were transformed into yeast to measure growth defects as in C. E-F.
760 Analytical scheme of primary deviation score (**E**) and secondary deviation score (**F**). Details are
761 in **Methods**.

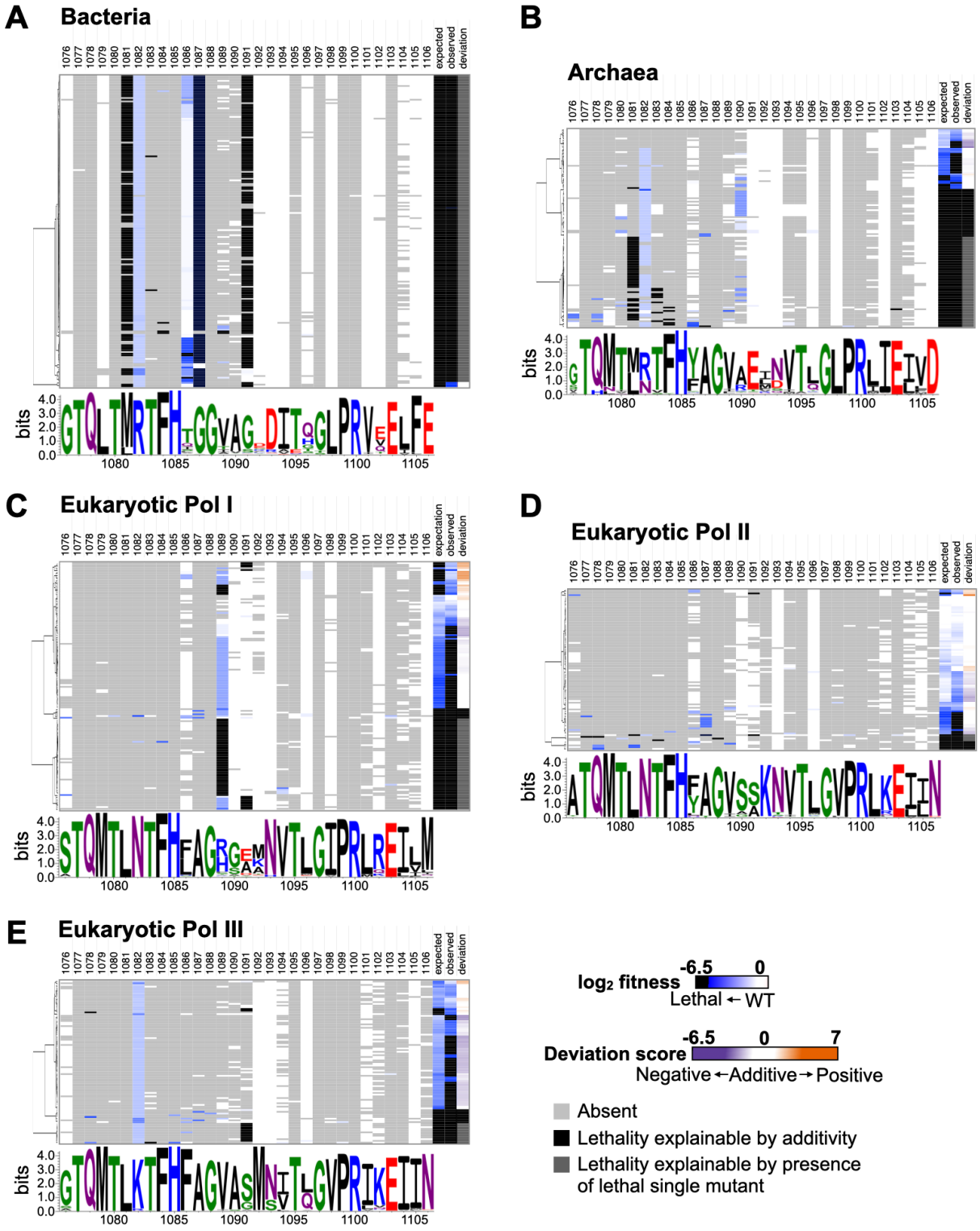
A
Bacteria
B
Archaea
C
Eukaryotic Pol I
D
Eukaryotic Pol II
E
Eukaryotic Pol III
expected
observed
deviation
bits
log2 fitness
-6.5
0
Lethal ← WT
Deviation score
-6.5
0
7
Negative ← Additive → Positive
Absent
Lethality explainable by additivity
Lethality explainable by presence of lethal single mutant

762

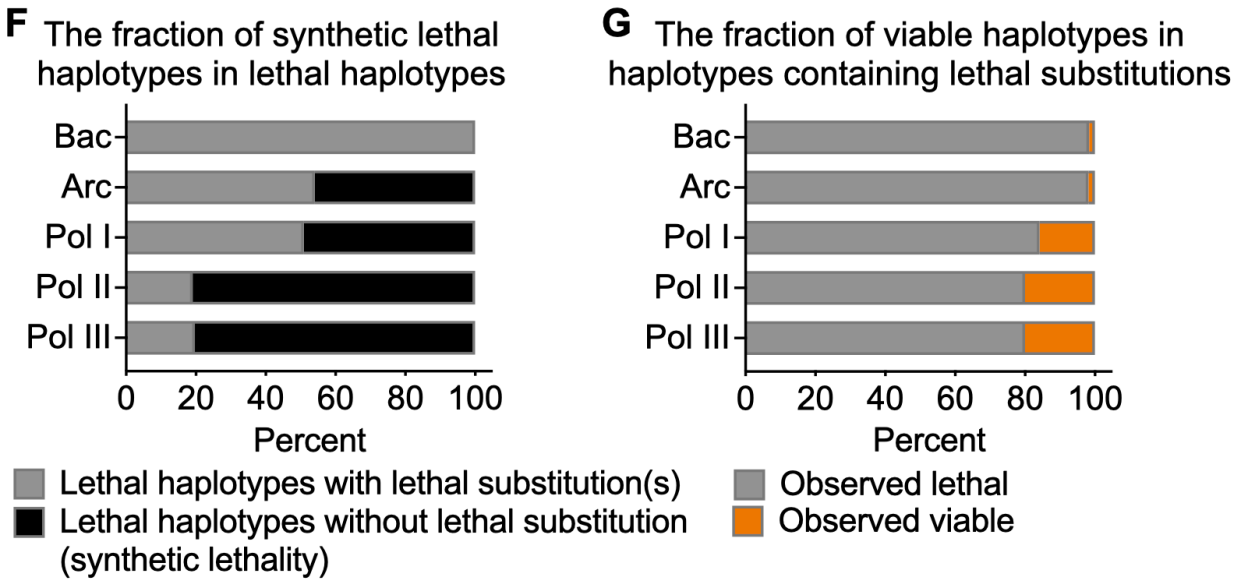

Figure 2. Greater TL-internal epistasis is observed with closer evolutionary distance to eukaryotic Pol II. A-E. Fitness and primary deviation score heatmaps of TL haplotypes from five msRNAP evolutionary groups. The *x*-axis of each heatmap is the 31 residue positions of the Pol II TL (1076-1106). The *y*-axis of each heatmap is the TL haplotypes belonging to each group clustered by hierarchical clustering with Euclidean distance. Each row represents one haplotype with several single substitutions. Light grey blocks in each row represent the residue from the haplotype at the position is the same with yeast Pol II TL residue, in other words, no substitution at the position. Colored blocks represent different residues in the haplotype compared with yeast Pol II TL (substitutions). The color of the block represents growth fitness of the single substitution in the yeast Pol II TL background. Expected fitness of the haplotypes were calculated from the log additive model for individual substitutions. Observed fitness was measured in the screening experiments, and deviation scores were calculated by comparing the observed and expected scores (shown at the right end of each row). Sequence logos were generated with multiple sequence alignment (MSA) of the five groups individually in Weblogo 3.7.12. The labeled numbers of the sequence logo represent yeast Pol II TL residue position (1076-1106). Bacteria n=465. Archaea n=426. Pol I n=605. Pol II n=405. Pol III n=444. **F**. Lethal haplotypes can contain three distinct types of lethality: one attributed to synthetic lethal interactions among substitutions, representing negative interactions that result in lethality beyond expectation, additive lethality expected from combination of individual substitutions, and that arising directly from the presence of an individually lethal single substitution. The calculated ratio specifically reflects the proportion of lethality due to negative interactions and additive lethality within all types of lethal haplotypes. **G**. The ratio of viable haplotypes in haplotypes containing lethal substitutions, representing the ratio of positive interactions (suppression) in TL haplotypes of each group. Haplotypes containing lethal substitutions are expected to be lethal based on the additive model. If haplotypes with lethal substitutions are observed to be viable, it suggests other substitutions suppress the lethal substitution in the haplotypes, implying positive epistasis (suppression). Approximately 20% of examined eukaryotic TL haplotypes containing individual lethal substitutions are viable, whereas only roughly 2% of bacterial and archaeal TL haplotypes are viable, suggesting positive interactions in eukaryotic TLs can buffer negative effects in more closely related TL sequences.

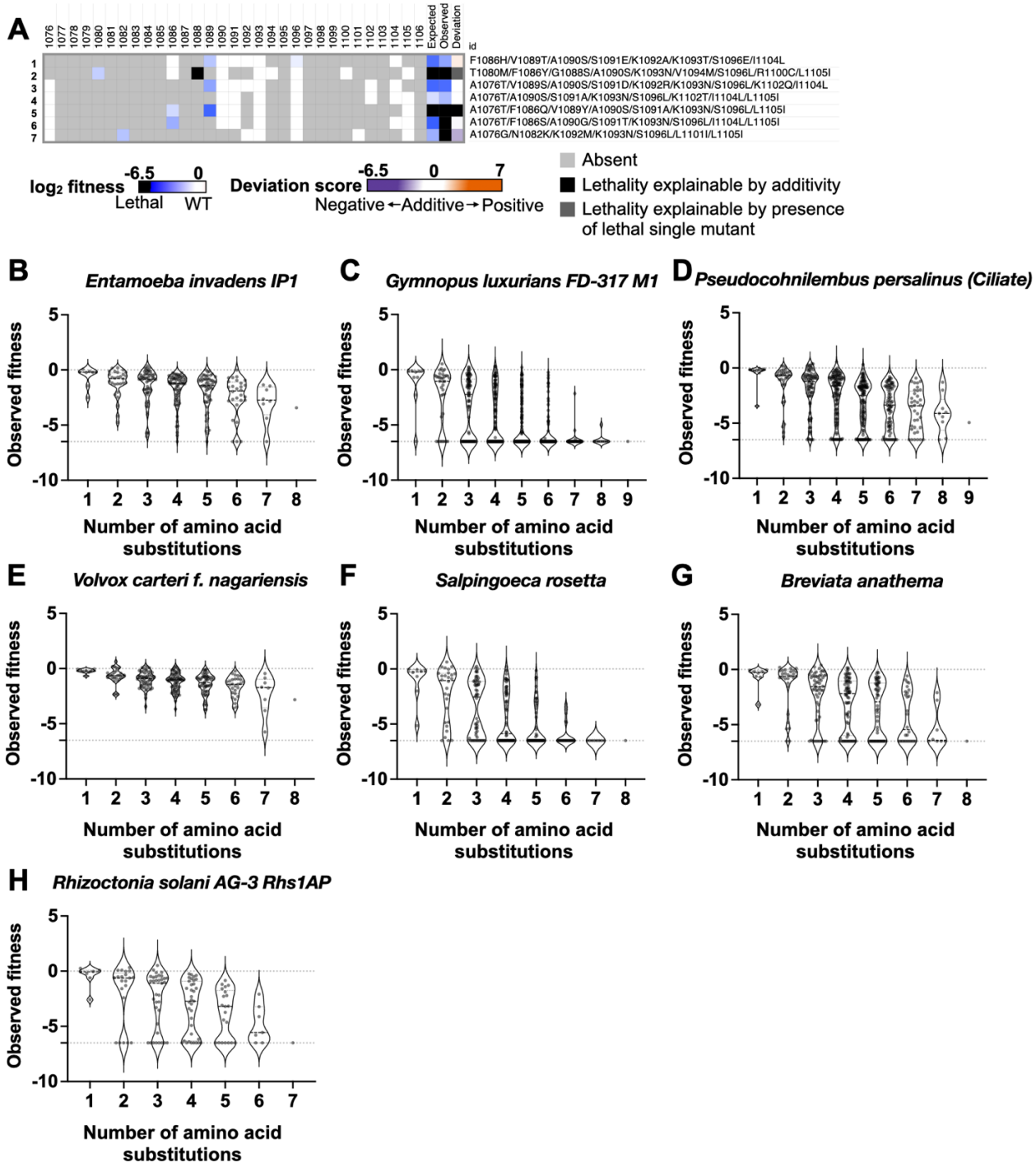

Figure 3. Phenotypes fluctuate with changes in substitution composition within haplotype groups. A. Fitness of constituent single substitutions, and expected and observed fitness of the haplotypes, and deviation score are shown in heatmap for the selected seven haplotypes. The deviations shown in the heatmap are the primary deviation scores calculated by comparing observed fitness to expected fitness. **B-H**. Distribution of growth fitness across all intermediate substitution combinations categorized by number of amino acid substitutions for

each selected TLs. Each spot on the graph represents a haplotype. The *y*-axis indicates the fitness of each haplotype. The *x*-axis indicates the number of amino acid substitutions within these haplotypes. For example, consider a point in **B**, which represents a haplotype from the substitution combination in the TL of *E. invadens IP1*. If the point is positioned at x=3, showing it contains three substitutions, and at y=-0.5, indicating a fitness value of -0.5 for this haplotype.

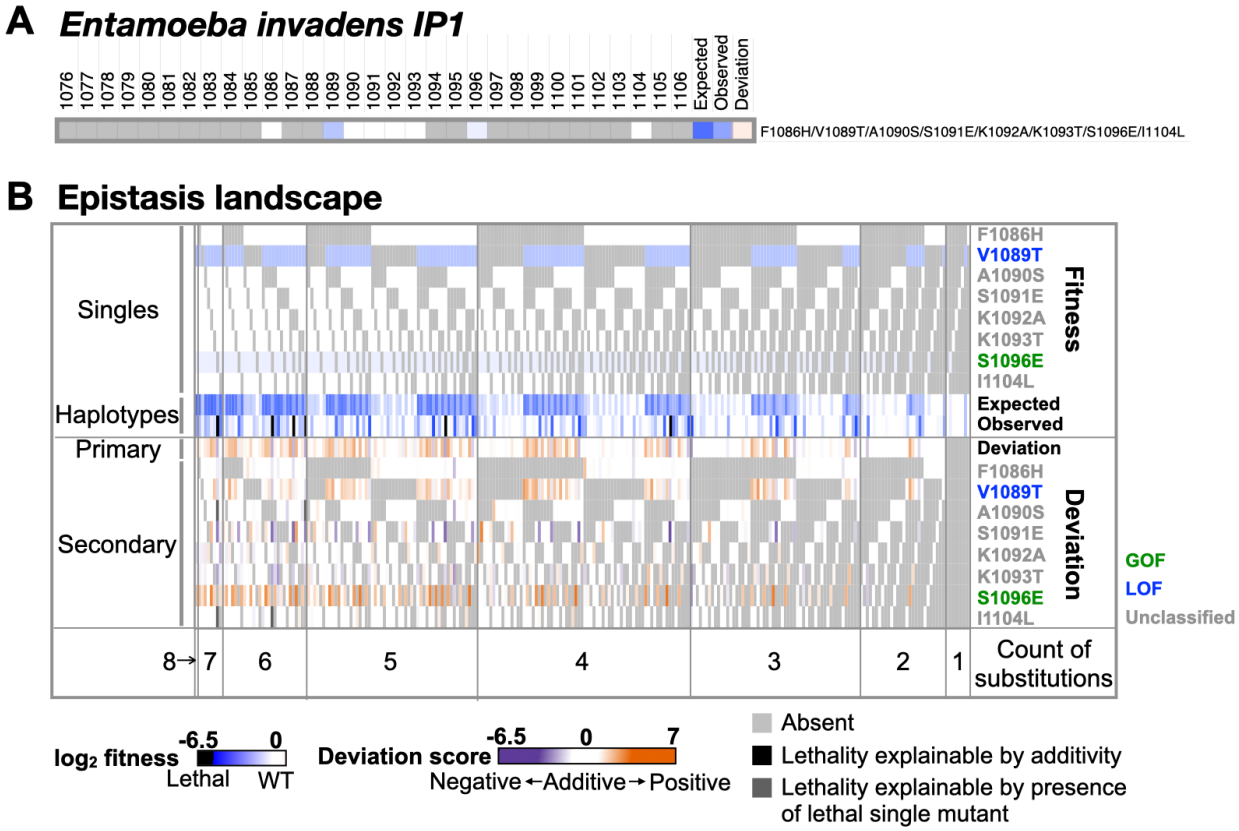

Figure 4. **The epistasis landscape provides a comprehensive view of primary and secondary deviation scores, emphasizing substitutions with notable epistatic effects. A**. Fitness of eight *Entamoeba invadens IP1* TL single substitutions in the yeast Pol II background, and the expected and observed fitness and the primary deviation score are shown in the heatmap. **B**. The epistasis landscape of *E. invadens IP1* TL substitutions. The heatmap illustrates the fitness and epistasis of all unique intermediate haplotypes coming from combinations of eight substitutions. Intermediate haplotypes are grouped by number of substitutions from 1 to 8. The fitness values are displayed in the upper panel and the epistasis, represented by primary and secondary deviation scores, is displayed in the lower panel. The colors of substitution names indicates their phenotype profiles as single mutants, GOF is in green, LOF is in blue, unclassified is in grey.

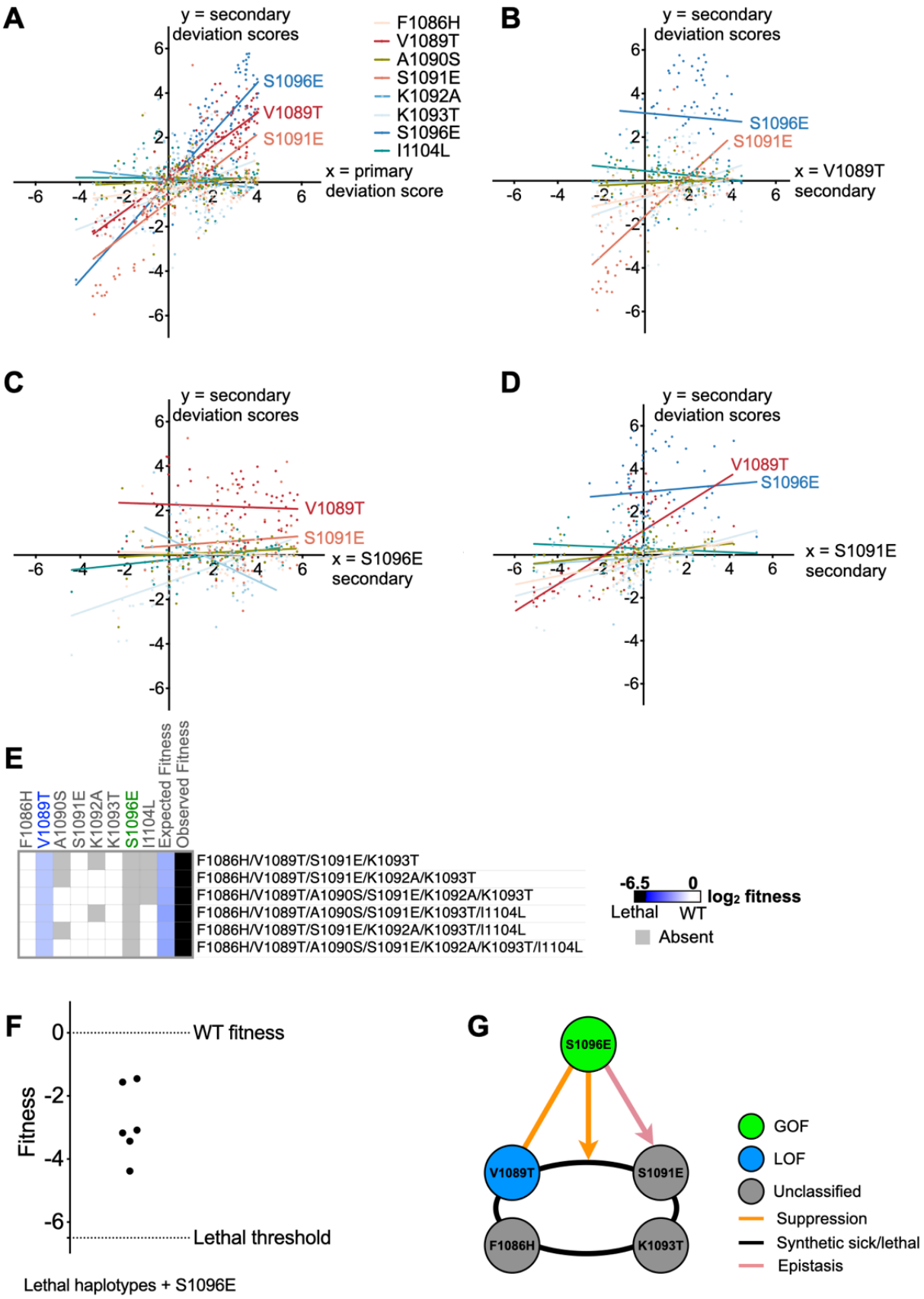
A
y = secondary deviation scores
x = primary deviation score
S1096E
V1089T
S1091E
F1086H
V1089T
A1090S
S1091E
K1092A
K1093T
S1096E
I1104L
B
y = secondary deviation scores
x = V1089T secondary
S1096E
S1091E
C
y = secondary deviation scores
x = S1096E secondary
V1089T
S1091E
D
y = secondary deviation scores
x = S1091E secondary
V1089T
S1096E
E
F1086H
V1089T
A1090S
S1091E
K1092A
K1093T
S1096E
I1104L
Expected Fitness
Observed Fitness
F1086H/V1089T/S1091E/K1093T
F1086H/V1089T/S1091E/K1092A/K1093T
F1086H/V1089T/A1090S/S1091E/K1092A/K1093T
F1086H/V1089T/A1090S/S1091E/K1093T/I1104L
F1086H/V1089T/S1091E/K1092A/K1093T/I1104L
F1086H/V1089T/A1090S/S1091E/K1092A/K1093T/I1104L
-6.5
0
log2 fitness
Lethal
WT
Absent
F
Fitness
WT fitness
Lethal threshold
Lethal haplotypes + S1096E
G
S1096E
V1089T
S1091E
F1086H
K1093T
GOF
LOF
Unclassified
Suppression
Synthetic sick/lethal
Epistasis

818

Figure 5. Correlations between deviation scores reflect specific residue interactions in *E. invadens IP1* TL substitutions. A. Correlations between secondary deviation scores of all eight substitutions (*y*-axis) and the primary deviation score (*x*-axis). Linear regression was applied to each comparison of secondary deviation scores against primary deviation scores to check the correlation. Substitutions with an R^2 value exceeding 0.5 are annotated on the *x*-*y* plot, indicating their substantial impact on primary epistasis of the haplotypes. **B-D**. Correlations between secondary deviations of the other seven substitutions (*y*-axis) vs V1089T (**B**), S1096E (**C**), S1091E (**D**) on the *x*-axes respectively. **E**. The fitness landscape of intermediate combinations with fitnesses in the ultra-sick/lethal range. Their observed fitness levels are in the lethal range as indicated with black blocks in the heatmap while the expected fitness scores calculated from the additive model is in viable range (light blue blocks), indicating potential negative interactions. The fitness scores of the constituent single mutants within lethal haplotypes are shown in the heatmap. F1086H, V1089T, S1091E, and K1093T are present in each lethal haplotype while S1096E is absent. Names of substitutions are colored based on their phenotype profiles as single mutants. GOF: green. LOF: blue. No obvious phenotype: grey. **F**. The fitness of all ultra-sick to lethal haplotypes with S1096E incorporated is no longer in the ultra-sick/lethal range. **G**. Scheme of specific residue interactions within substitutions of *E. invadens IP1* TL.

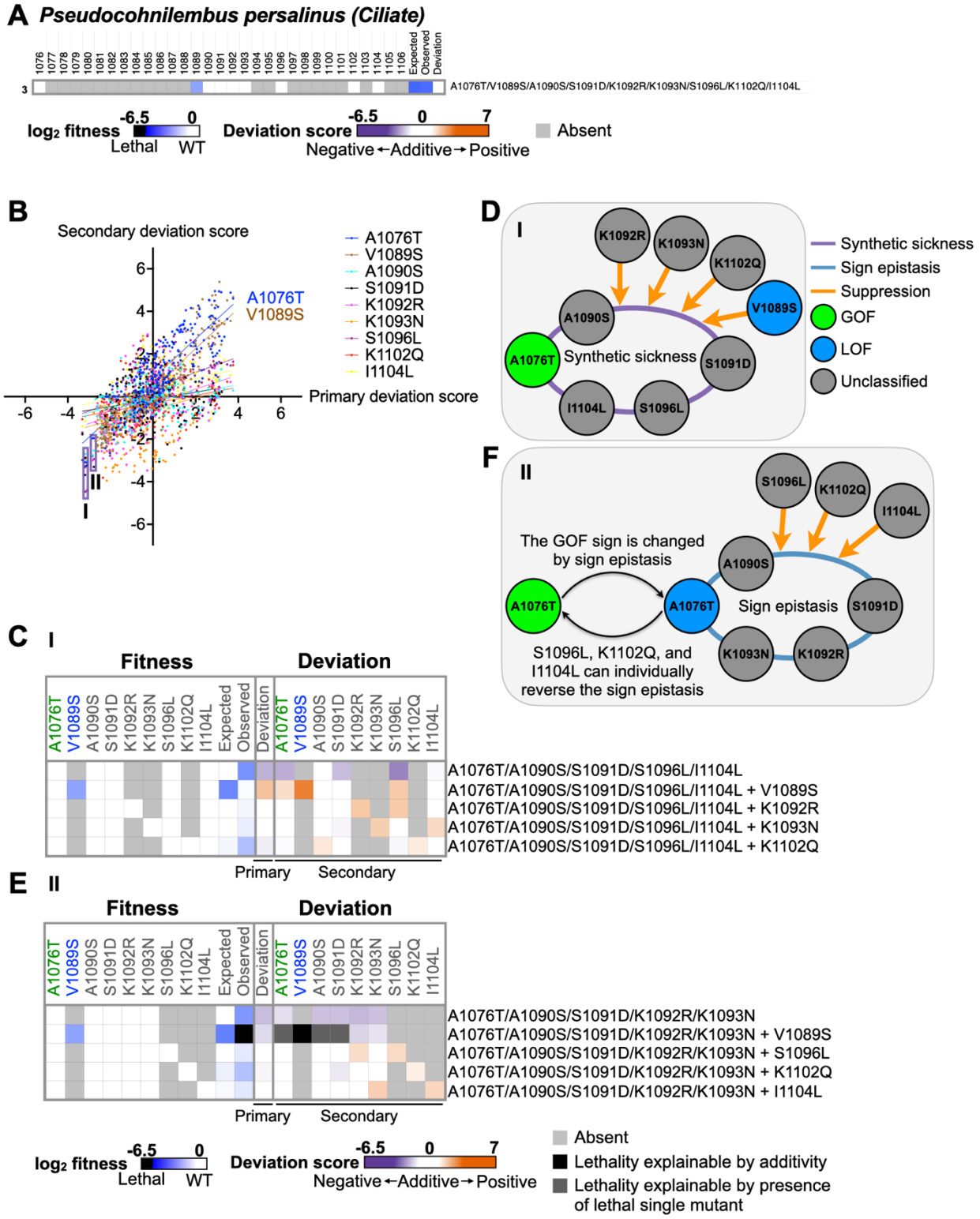

Figure 6. Intricate higher-order epistasis observed in substitutions of *P. persalinus (Ciliate)* TL haplotype. A. The heatmap displays the fitness of nine single substitutions in *P. persalinus (Ciliate)* TL in the yeast Pol II background, along with the epistasis between them represented by the primary deviation score. **B**. Similar to Fig. 5A, we checked correlations

842 between secondary deviation scores (*y*-axis) to the primary deviation score (*x*-axis) to identify
843 substitutions with substantial impact on primary deviation scores. Simple linear regression was
844 applied to each comparison. Substitutions with $R^2 > 0.5$ are annotated in the plot. **C**. The fitness
845 and deviation scores of substitution combinations related to group I are shown in the heatmap.
846 Names of substitutions are colored based on their phenotypic profiles as single mutants. GOF:
847 green. LOF: blue. No obvious phenotype (unclassified): grey. Each line shows the fitness and
848 deviation scores of substitutions in a certain combination. Left, the fitness of individual
849 substitutions, and the expected and observed fitness. Right, the primary deviations calculated
850 by comparing observed and expected fitness and the secondary deviation scores of each
851 constituent substitution. A1076T/A1090S/S1091D/S1096L/I1104L is in the first line. Its observed
852 fitness is smaller than expected and when compared, resulting in a negative primary deviation
853 score, representing a negative interaction. The secondary deviation scores of each constituent
854 substitutions are all negative, indicating each of them showing negative interactions when
855 adding to corresponding compounds. The following four lines represent the four combinations
856 where V1089S, K1092R, K1093N, and K1102Q are incorporated into
857 A1076T/A1090S/S1091D/S1096L/I1104L respectively. All observed fitness of combinations is
858 healthier than A1076T/A1090S/S1091D/S1096L/I1104L, and the secondary deviation scores of
859 V1089S, K1092R, K1093N and K1102Q are all positive, implying positive effect (suppression)
860 on each combination respectively. **D**. Scheme illustrating the substitution interaction network
861 observed in C. **E**. Similar to C, the fitness and deviation scores of combinations related with
862 group II are shown in the heatmap. The first row shows the fitness and deviation scores
863 detected within the combination A1076T/A1090S/S1091D/K1092R/K1093N. The following rows
864 displays the corresponding fitness and deviation scores when the other four substitutions are
865 incorporated. Notably, the effect of V1089S on A1076T/A1090S/S1091D/K1092R/K1093N
866 cannot be determined because the observed fitness of the combination (V1089S +
867 A1076T/A1090S/S1091D/K1092R/K1093N) is in the ultra-sick/lethal range, and its expected
868 fitness calculated from the log additive model is also in the lethal range due to additivity. In this
869 case, the secondary deviation of V1089S is represented by a black block in the heatmap.
870 Moreover, the effect of A1076T on V1089S/A1090S/S1091D/K1092R/K1093N cannot be
871 determined because the observed fitness falls within the lethal range. The expected fitness of
872 (A1076T + V1089S/A1090S/S1091D/K1092R/K1093N) is also in the lethal range due to the
873 presence of the lethal compound V1089S/A1090S/S1091D/K1092R/K1093N. The expected
874 lethality of the combination is because it contains a lethal component. The secondary deviation
875 score of A1076T cannot be determined either and is indicated by a dark gray block in the
876 heatmap. Similarly, the scores of A1090S and S1091D could not be determined for the same
877 reason with A1076T and are also marked with dark grey blocks. **F**. Scheme representing the
878 substitution interaction networks observed in E.

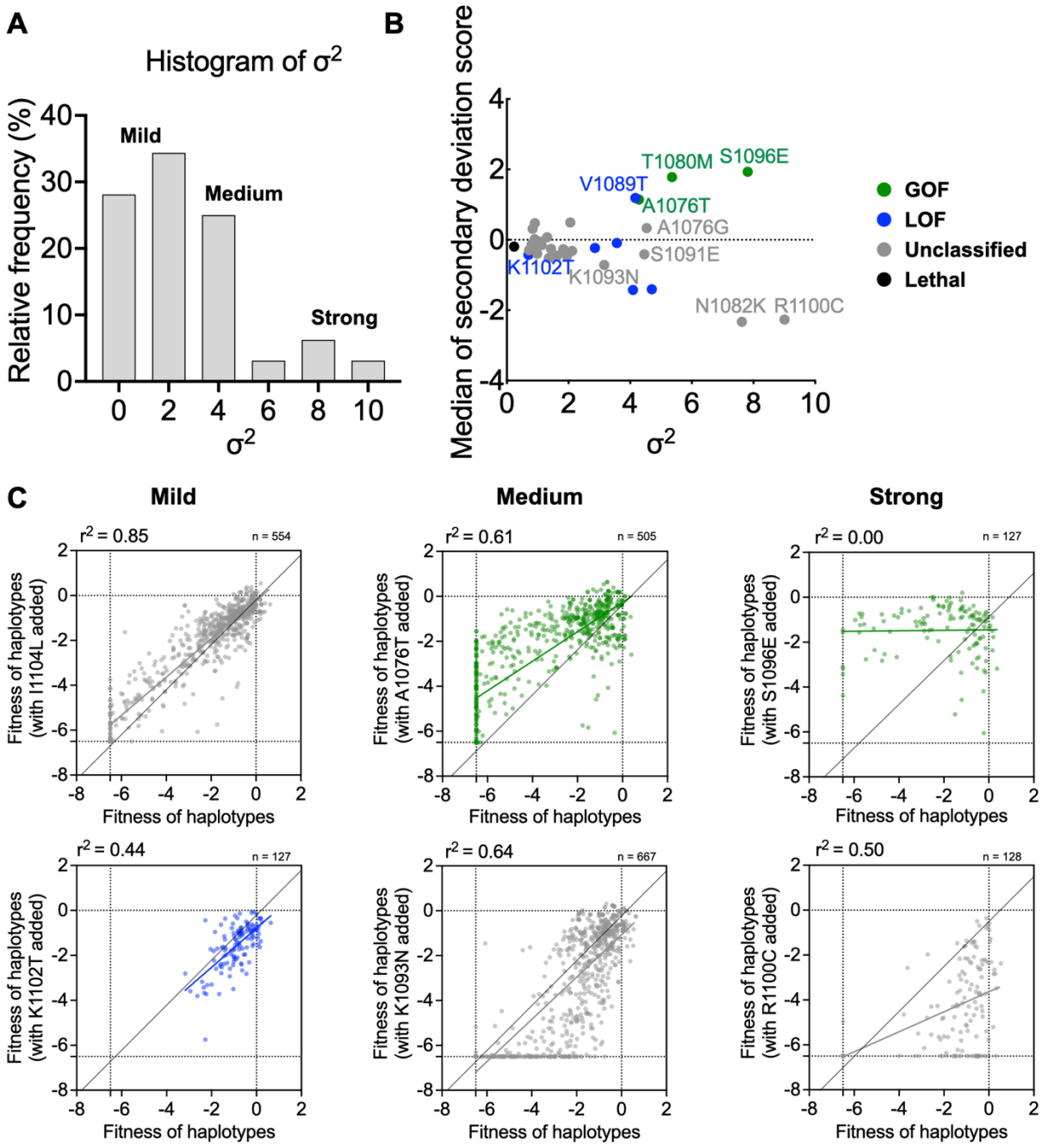

Figure 7. Different classes of epistatic effects. A. Histogram of mutants' epistatic effects, represented by their respective maximum likelihood estimate (σ^2) of secondary deviation scores. Higher epistatic effect indicates greater impact of a certain substitution. **B**. Medians of secondary deviation scores of substitutions were plotted against their corresponding σ^2. Substitutions are colored based on their phenotypes. **C**. Comparing epistatic effects of mutants in each category. Each scatter plot shows the measured fitness of haplotypes without (*x*-axis) versus with (*y*-axis) a substitution incorporated. The colors of the plots represent the mutants' phenotypes. The colored line marks the simple linear regression of the spots, representing the observed epistatic effect of the substitution. R^2 values of the regressions are labeled in the plots. The black line indicates the additive (non-epistatic) expectation.

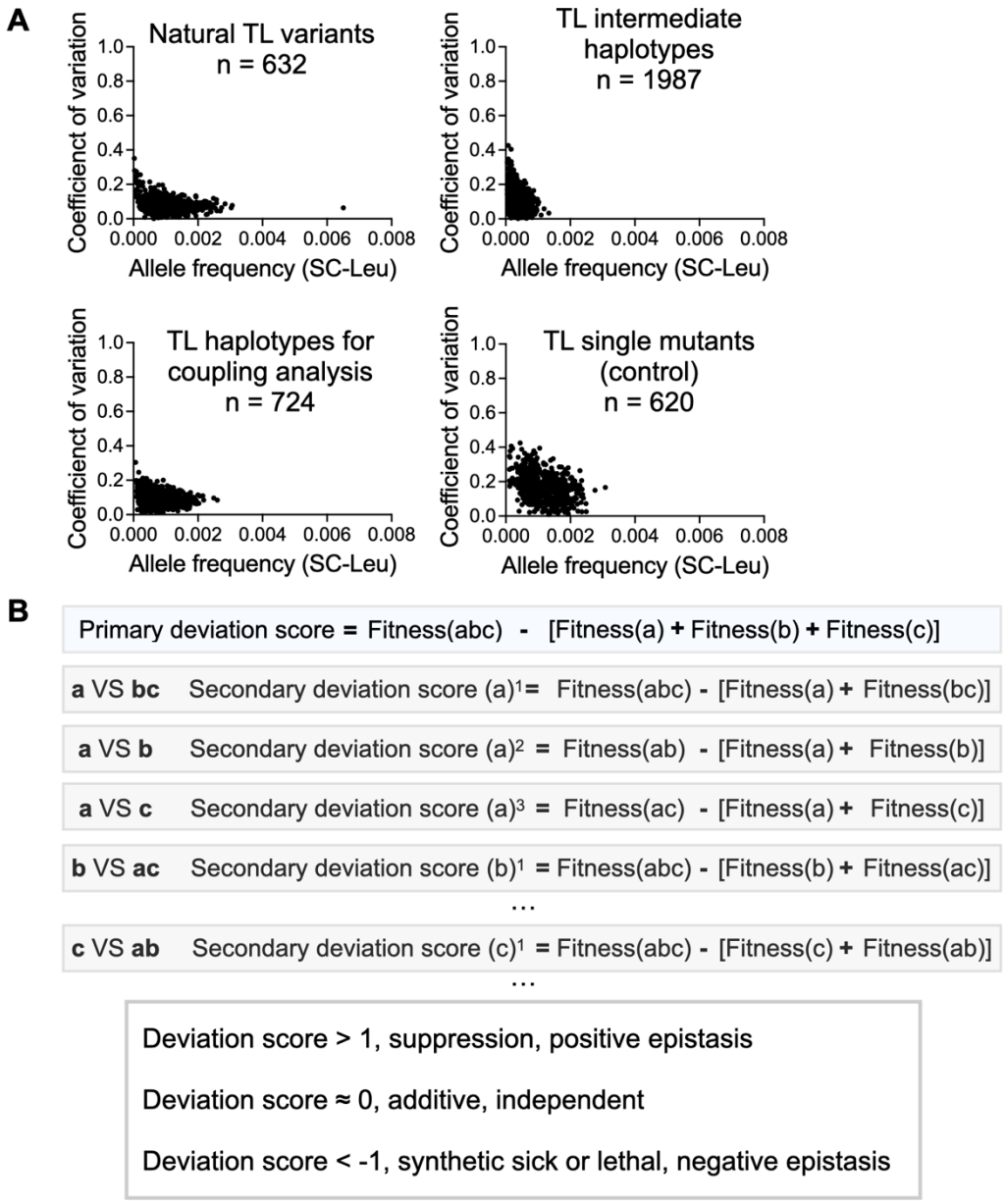

Figure S1. Detection of higher-order interactions by primary and secondary deviation scores. A. The low coefficients of variation for all libraries involved in this study indicate high reproducibility across the datasets. The coefficient of variation is plotted against the allele frequency in the control condition, SC-Leu, for each of the four libraries. **B**. For a pseudo haplotype “abc”. The primary deviation score is calculated by comparing the observed fitness of the haplotype to the log additive of constituent substitutions’ fitness. The secondary deviation score of “a” in “abc” represents the epistatic effect of “a” on “bc” and is calculated by comparing the observed fitness score of “abc” to the additive of fitness scores of “a” and “bc”. The secondary deviation score of “a” in “ab” represents the epistatic effect of “a”on “b”. It is calculated by comparing the observed fitness score of “ab” to the additive of fitness scores of “a” and “b”. If the deviation score ≈ 0, it indicates the constituent substitutions are independent and there is no interaction among them. If the deviation score > 1, it represents positive

904 epistasis (suppression) among the constituent substitutions. If the deviation score < -1, it
905 represents negative epistasis (synthetic sickness or lethality) among the constituent
906 substitutions.

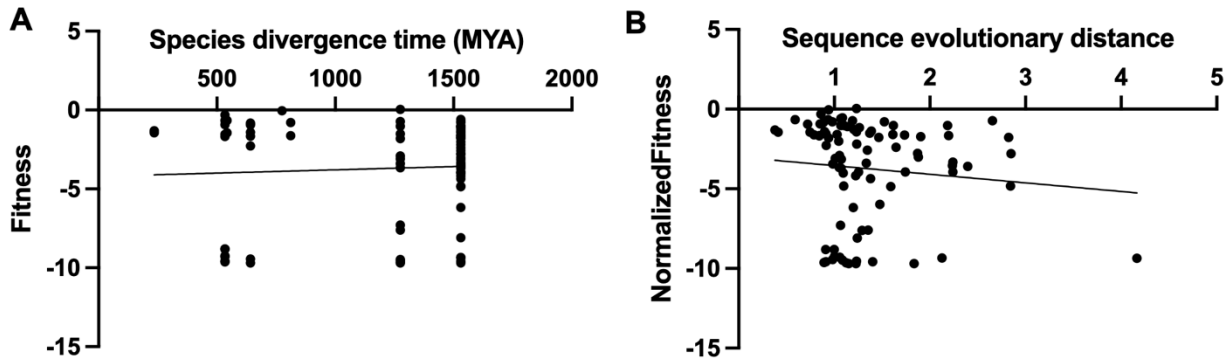

Figure S2. Evolutionary distances do not correlate with the growth fitness of TL haplotypes. A. The divergence time between the species from which the TL haplotypes originate and the yeast *Saccharomyces cerevisiae*, which contains the WT TL, does not correlate with the fitness of the Pol II TL haplotypes. The median divergence times showing in *x*-axis are represented with millions of years ago (MYA) and calculated by TimeTree5 (KUMAR *et al.* 2022). The line represents the simple linear regression between the divergence time and the fitness: $y = 0.0004123 * x - 4.201$ (slope is not significantly different from zero). **B**. The evolutionary distance between the genes that the Pol II TL haplotypes are from and the yeast *RPB1* gene, which contains the WT TL, does not correlate with growth fitness. The sequence evolutionary distances are calculated by MEGA11 with JTT model (TAMURA *et al.* 2021). The line represents the simple linear regression between the evolutionary distance and the fitness: $y = -0.5401 * x - 3.005$ (slope is not significantly different from zero).

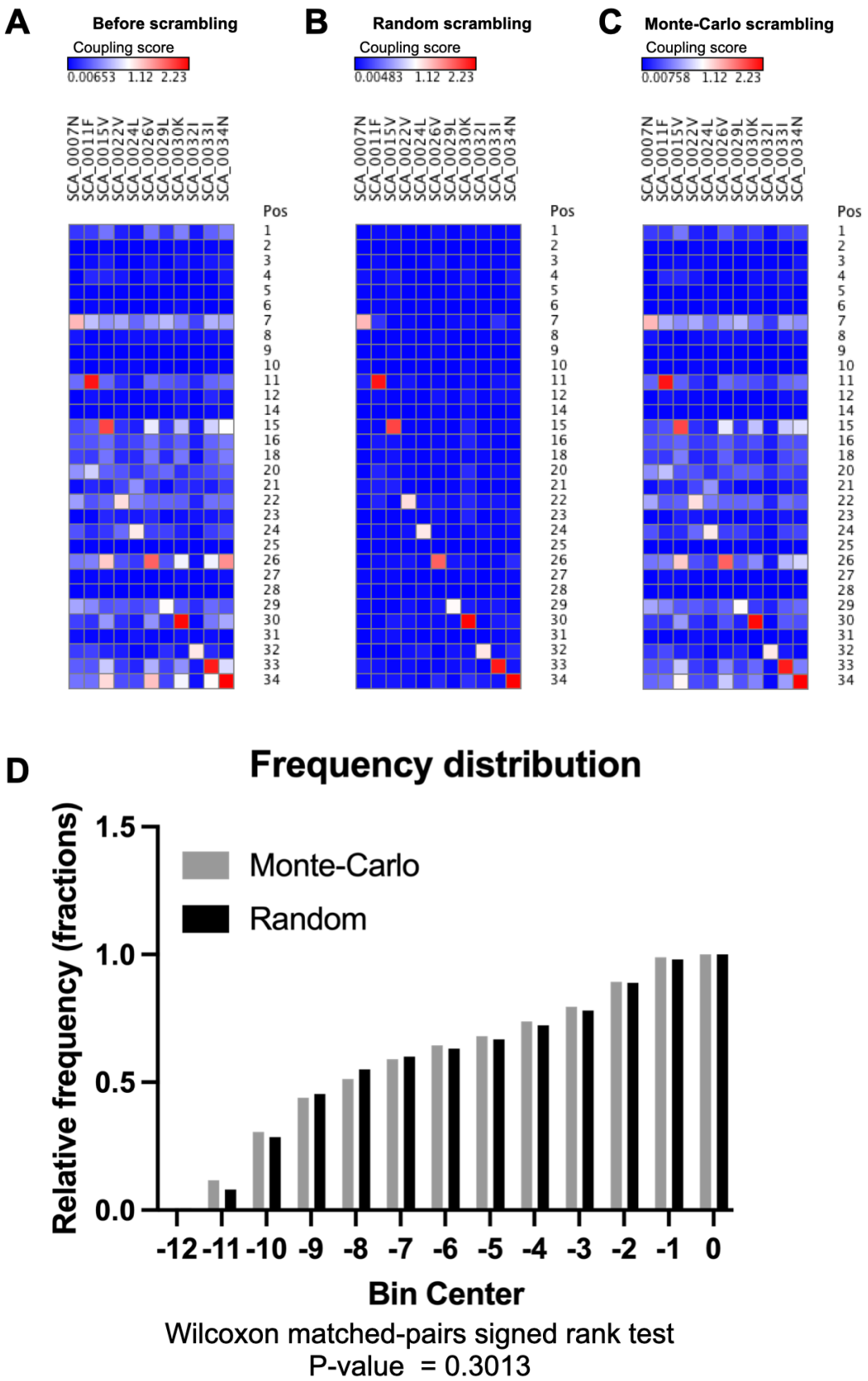
A
Before scrambling
Coupling score
0.00653 1.12 2.23
B
Random scrambling
Coupling score
0.00483 1.12 2.23
C
Monte-Carlo scrambling
Coupling score
0.00758 1.12 2.23
SCA_0007N
SCA_0011F
SCA_0015V
SCA_0022V
SCA_0024L
SCA_0026V
SCA_0029L
SCA_0030K
SCA_0032I
SCA_0033I
SCA_0034N
Pos
D
Frequency distribution
Monte-Carlo
Random
Relative frequency (fractions)
1.5
1.0
0.5
0.0
-12 -11 -10 -9 -8 -7 -6 -5 -4 -3 -2 -1 0
Bin Center
Wilcoxon matched-pairs signed rank test
P-value = 0.3013

921

922

923 **Figure S3. Design of mutant libraries to assess TL-internal residue coupling. A**. Residue
924 coupling heatmaps of natural TL variants. Statistical coupling analysis of TL multiple sequence
925 alignment including 362 selected natural eukaryotic Pol I, II, and III TL alleles. **B-C**. Heatmaps of
926 coupled residues in Random scrambling and Monte Carlo scrambled haplotypes. The random
927 scrambling disrupted coupled residues in selected TL variants (**B**) while the Monte Carlo
928 scrambling haplotypes reserved coupled residues (**C**). **D**. Cumulative fitness frequency
929 distribution of the Random scrambling and Monte Carlo scrambling haplotypes. The Wilcoxon
930 matched-pairs signed rank test was used to assess the significance of the fitness distribution
931 difference between Monte Carlo scrambling and Random scrambling haplotypes. The P-value
932 indicates that they are slightly but significantly different.

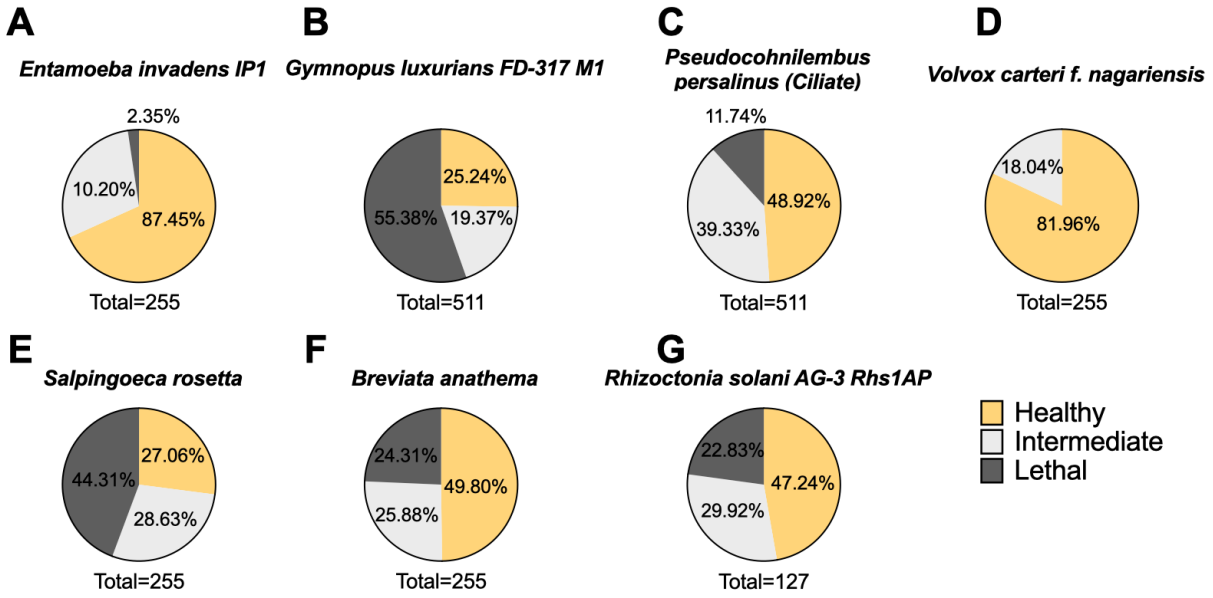

Figure S4. The percentage of fitness categories of all intermediate combinations within each haplotype (A-G). Healthy: Fitness > -2. Intermediate: -6.5 < Fitness ≤ -2. Lethal: Fitness ≤ -6.5.

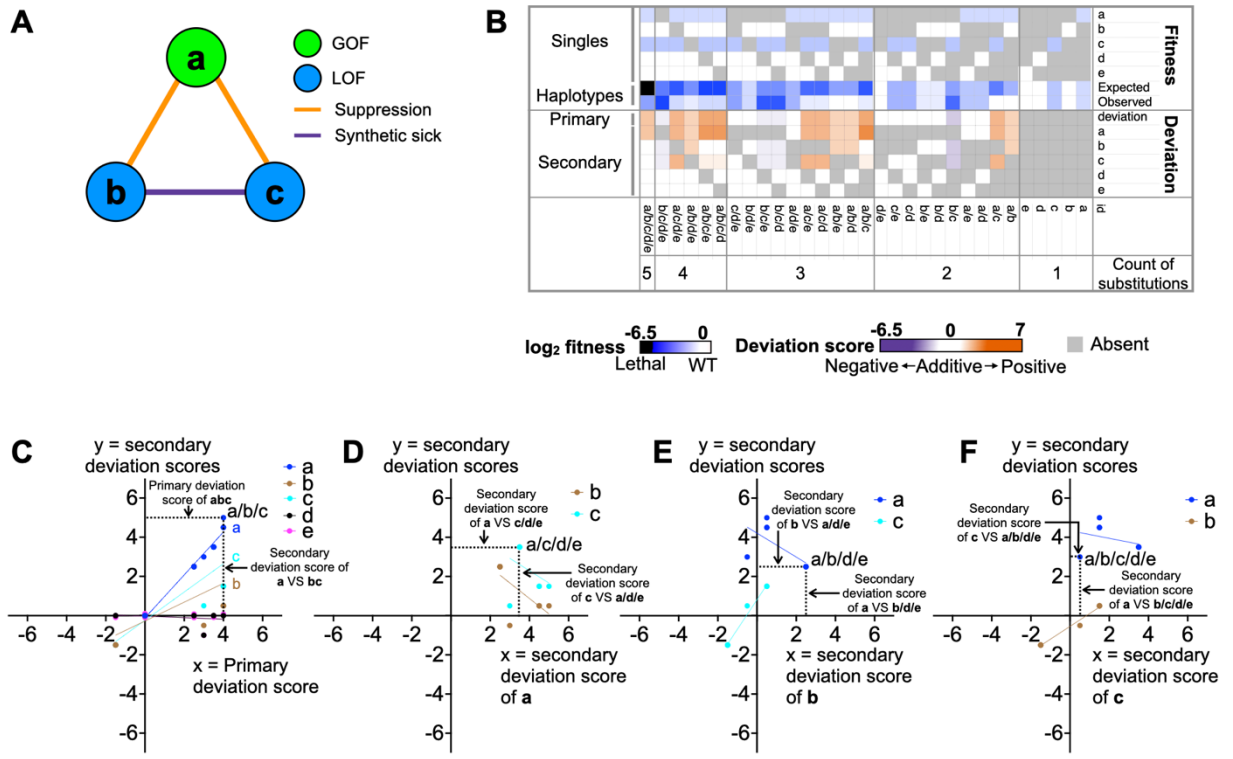

Figure S5. Example primary and secondary deviation scores for a simplified, simulated TL haplotype "abcde". A. Simulated interactions among substitutions "a", "b", and "c". We set the single mutant "a" as a GOF mutant, "b" and "c" as LOF mutants, while "e" and "f" have no effects. We also set suppression between GOF and LOF combinations ("ab" and "ac"), and synthetic sickness between LOF and LOF combinations ("bc"). **B**. The epistasis interaction landscape of simplified TL haplotype "abcde", illustrating the observed and expected fitness of all single substitutions and all intermediate haplotypes, as well as primary and secondary deviation scores in the simulation. **C**. Correlations between secondary deviation scores of all five single substitutions (*y*-axis) to the corresponding primary deviation scores (*x*-axis). To measure the correlation, linear regression was applied for secondary deviation scores of "a", "b", "c", "d", "e" to the corresponding primary deviations scores, respectively. Single substitutions with strong correlations ($R^2 > 0.5$) were labeled in the plot. Three substitutions with phenotypes show strong correlations in the simulation, "a", "b", and "c". **D-F**. The correlation between secondary deviation scores of the four substitutions (*y*-axis) vs "a" (**D**), "b" (**E**), "c" (**F**) on *x*-axis respectively. To read the plot, with **D** as an example, each cyan spot represents an intermediate combination containing both "a" and "c". The labeled spot represents a specific combination "a/c/d/e". Its coordinate value in *x*-axis represents the secondary deviation score of "a" to "c/d/e". Its coordinate value in *y*-axis represents the secondary deviation score of "c" to "a/d/e". We did a linear regression for all the cyan spots to represent the correlation between the secondary deviation scores of "c" to "a". This correlation helps illustrate the potential interaction between "c" and "a". The secondary deviation scores of "c" are all positive when "a" is present, meaning "c" constantly shows positive secondary score when "a" is present, indicating potential suppression of "c" to "a".

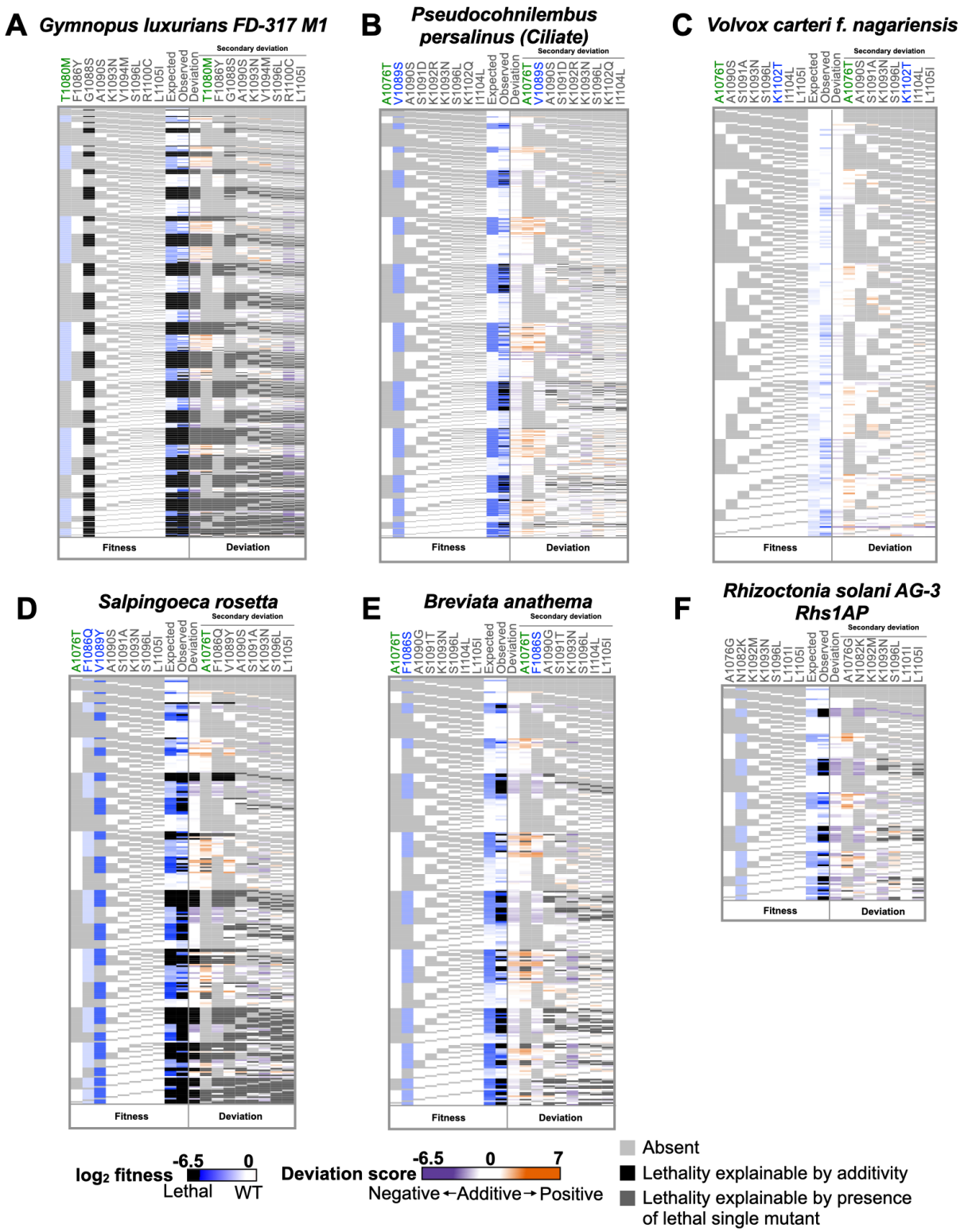

Figure S6. The epistasis landscapes of selected haplotypes. The fitness and epistasis of all unique intermediate haplotypes from combinations of substitutions within each haplotype (**A-F**). The colors of mutants' names represent mutants' phenotypes. GOF is in green, LOF is in green, non-classified mutants is in grey.

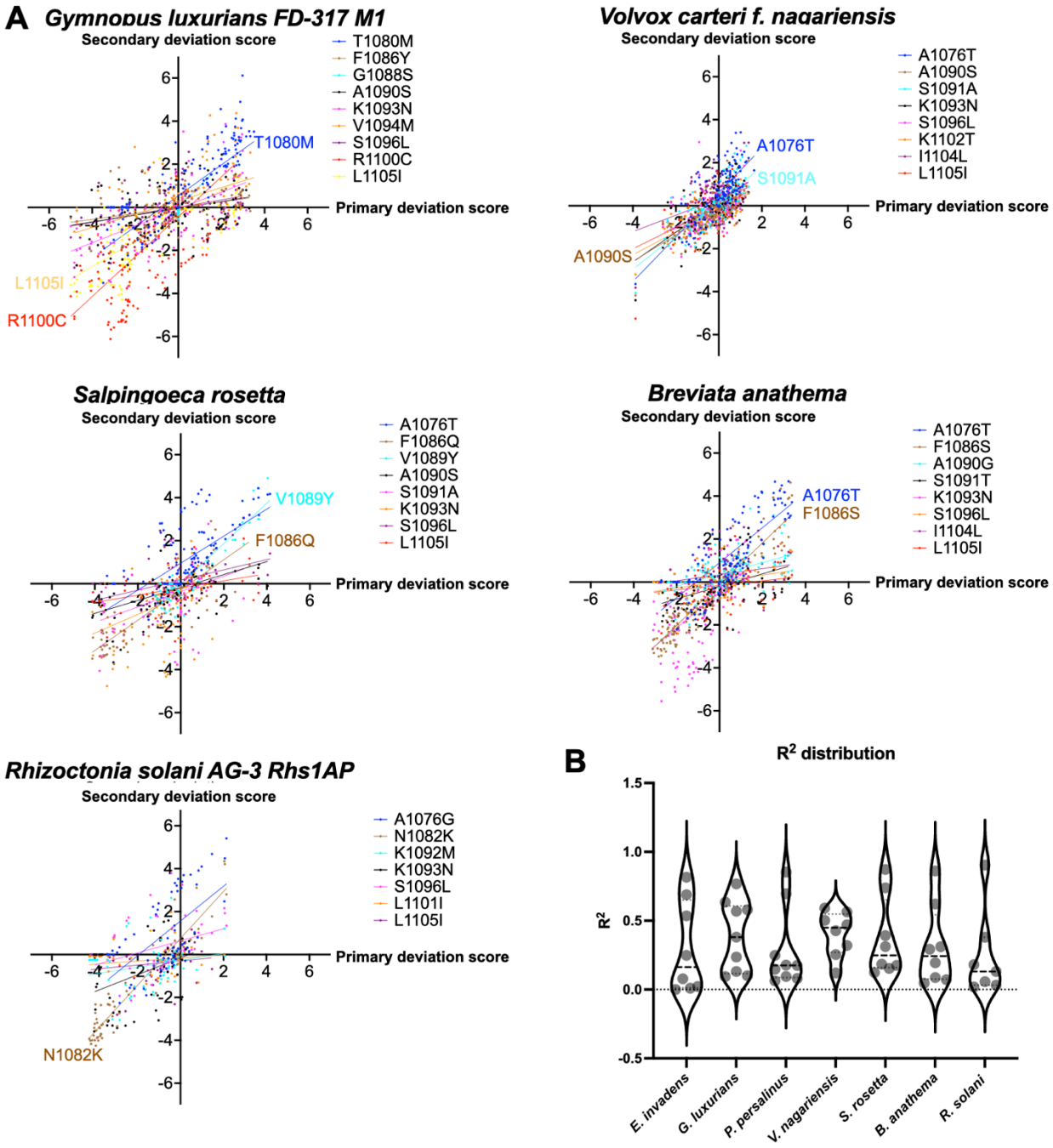

Figure S7. The epistasis within haplotypes is driven by several specific substitutions. A. The correlations between secondary deviation scores of all substitutions (*y*-axis) and the primary deviation score (*x*-axis) for each selected haplotype. Linear regression was applied to each comparison of secondary to primary deviation scores. Substitutions with R^2 value exceeding 0.5 are annotated on the *x*-*y* plot, indicating their substantial impact on primary epistasis of the haplotypes. **B**. Distributions of R^2 of all selected TL haplotypes.

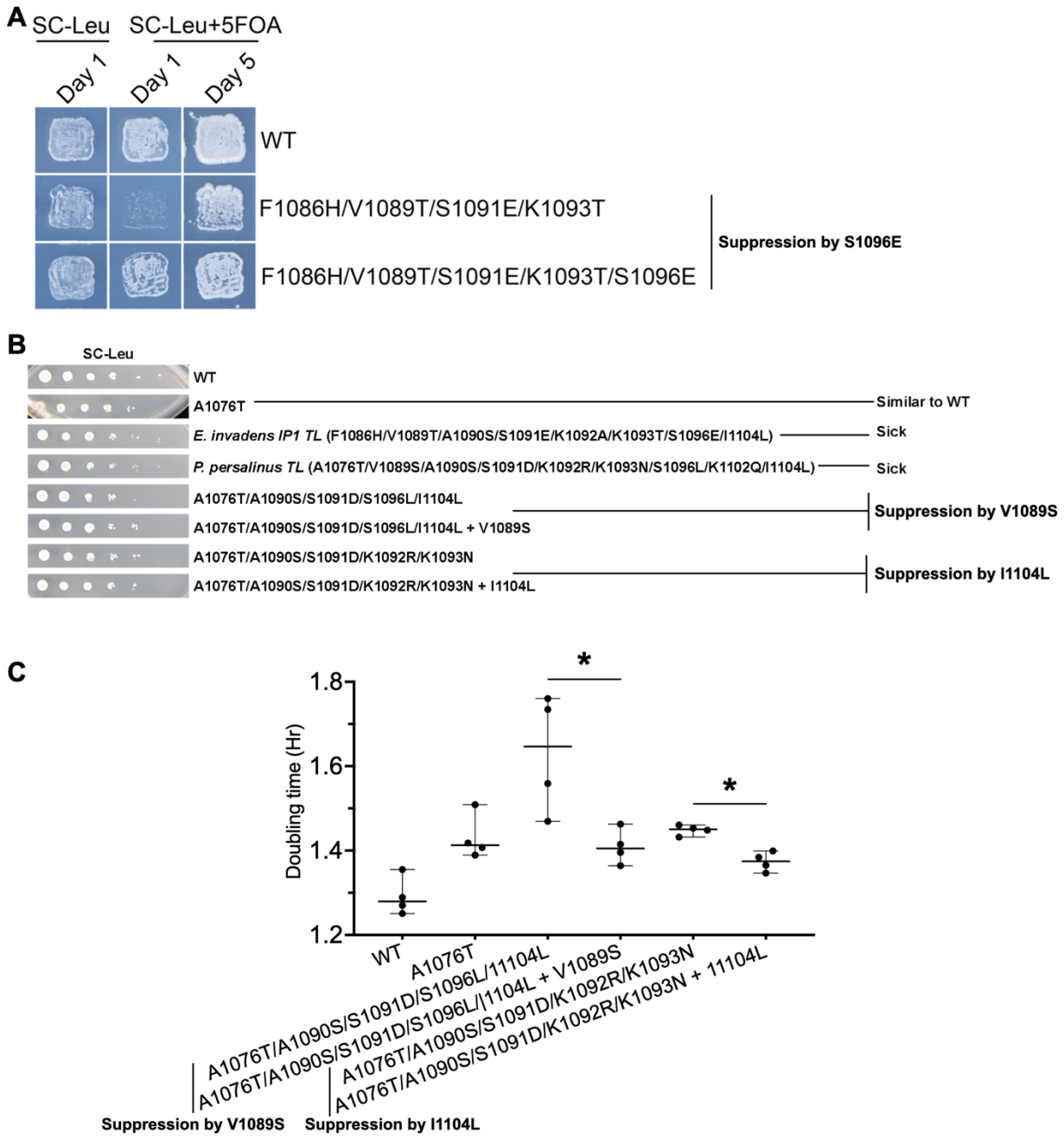

Figure S8. Validation of genetic interactions. Validating genetic interactions observed in high throughput libraries with growth assays. Haplotypes involved here were synthesized and transformed into WT yeast cells, and their sequencies were extracted and verified by sequencing. **A**. Confirmation of the suppression between S1096E and the synthetic sick/lethal group F1086H/V1089T/S1091E/K1093T by patch assay. Growth of patches on SC-Leu+5FOA indicates the growth defects of the haplotypes. F1086H/V1089T/S1091E/K1093T barely grew on SC-Leu+5FOA condition on Day 1, while F1086H/V1089T/S1091E/K1093T/S1096E showed near WT level growth, suggesting the suppression between S1096E and F1086H/V1089T/S1091E/K1093T. **B**. Verification of growth defects and genetic interactions in haplotypes and combinations by spot assay. The growth defects of *E. invadens* IP1 TL and *P.*

990 *persalinus* TL were confirmed by their smaller spot sizes compared to the WT, consistent with
991 our observations from the high throughput experiment. To validate the suppression interactions
992 observed in the high throughput data, we selected two pairs of haplotypes. While suppression
993 was detected in the spot assay, the interactions appeared more subtle. We further measured
994 their doubling times through growth curve assay in (**C**). **C**. Doubling time measurements
995 validated the suppression interactions observed in high throughput data. The doubling times are
996 significantly different in both suppression groups. TL variants were tested in four biological
997 replicates, each with three or four technical replicates. The median and 95% confidence interval
998 of each variant are shown in the figure. Kolmogorov-Smirnov test was performed to determine
999 whether the differences in doubling time among the haplotypes showing suppression were
1000 significant. The tests resulted in a P-value of 0.0286 in both comparisons, indicating statistically
1001 significant differences. The details of growth curve experiment are in **Methods**. Specific
1002 doubling times are provided in **Supplemental Table 1**.

1003

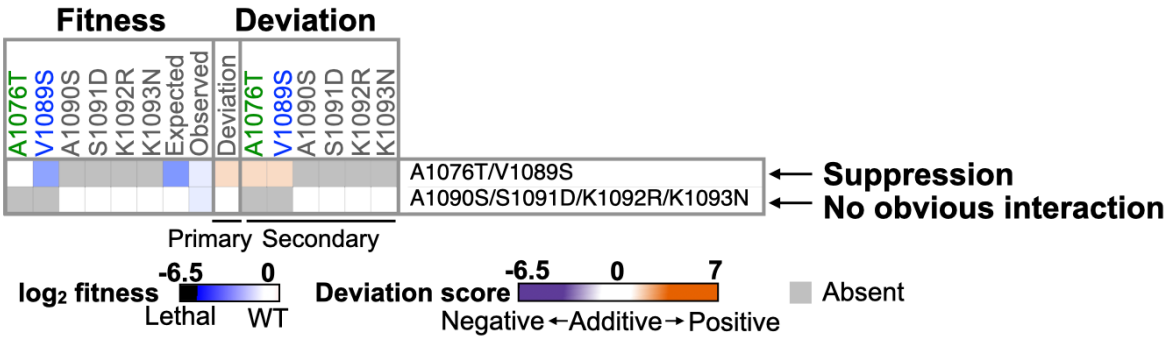

1004

1005 **Figure S9. Heatmap displaying fitness and deviation scores in A1076T/V1089S and**
1006 **A1090S/S1091D/K1092R/K1093N.** Positive deviation scores in A1076T/V1089S indicate
1007 suppression, and no deviations (primary and secondary deviation scores are around zero)
1008 indicate no interactions within A1090S/S1091D/K1092R/K1093N.

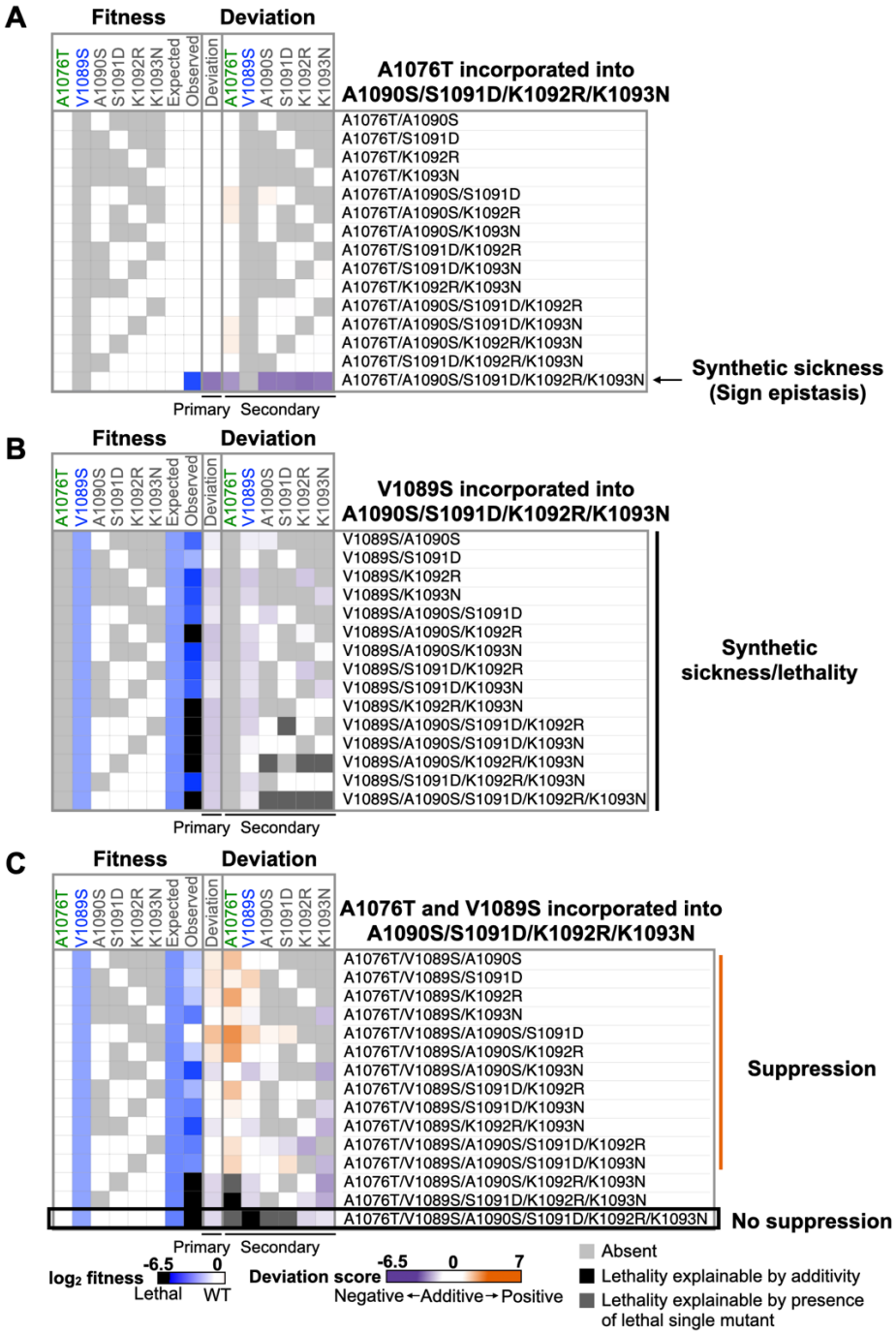

Figure S10. A1076T showed sign epistasis with A1090S/S1091D/K1092R/K1093N. A. Heatmap displays fitness and deviation scores for A1076T in all single substitutions and combinations with A1090S, S1091D, K1092R, K1093N, suggesting A1076T only showed negative interaction with A1090S/S1091D/K1092R/K1093N. **B**. Heatmap shows fitness and deviation scores for V1089S in all single substitutions and combinations with A1090S, S1091D, K1092R, K1093N. V1089S showed negative interactions with almost all of them. **C**. Heatmap shows fitness and deviation scores for A1076T and V1089S in all single substitutions and combinations with A1090S, S1091D, K1092R, K1093N. Positive interactions were observed in most combinations.

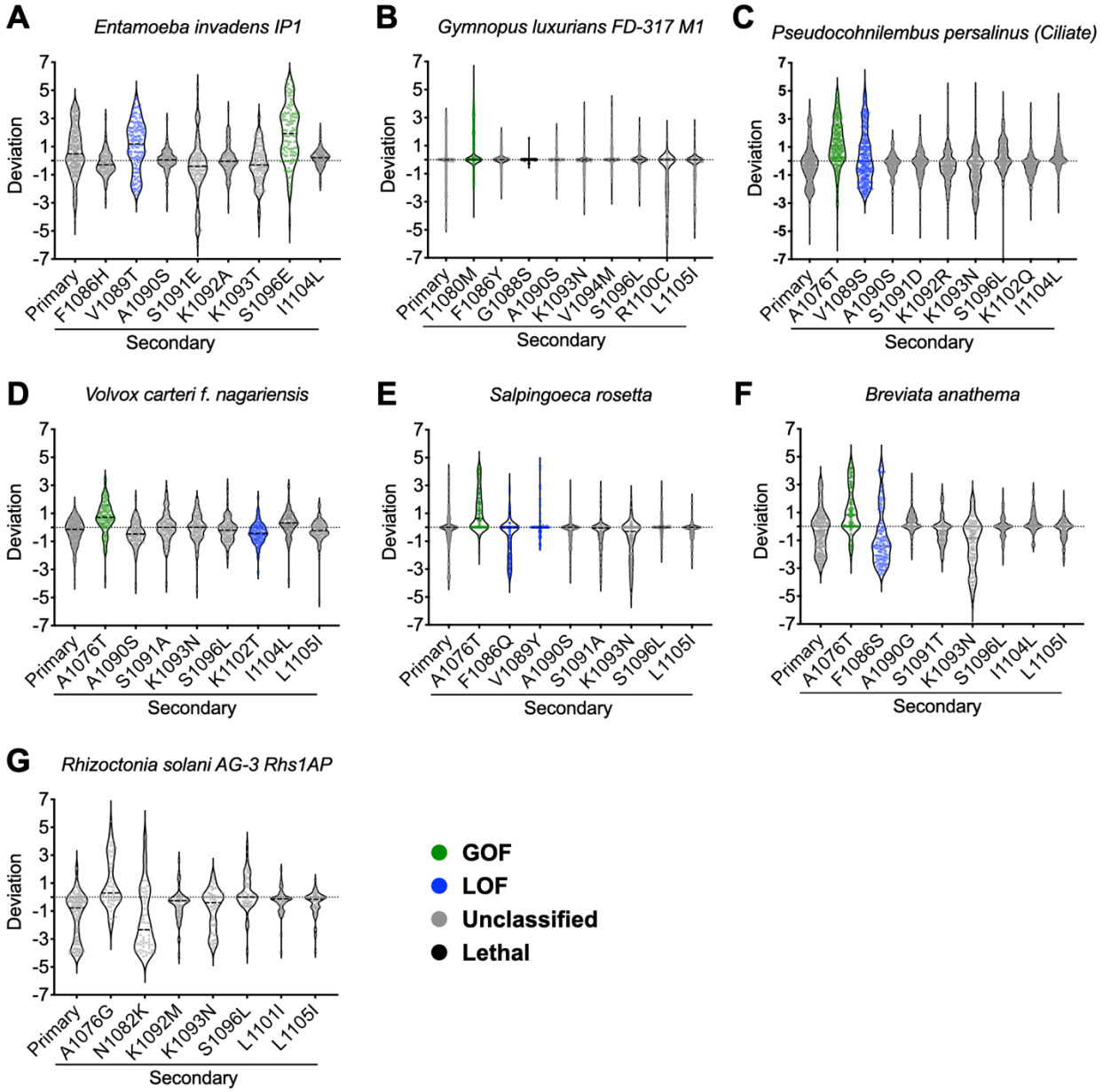

Figure S11. The distributions of primary and secondary deviation scores within each selected haplotype (A-G). Colors of spots represent phenotypes of substitutions.

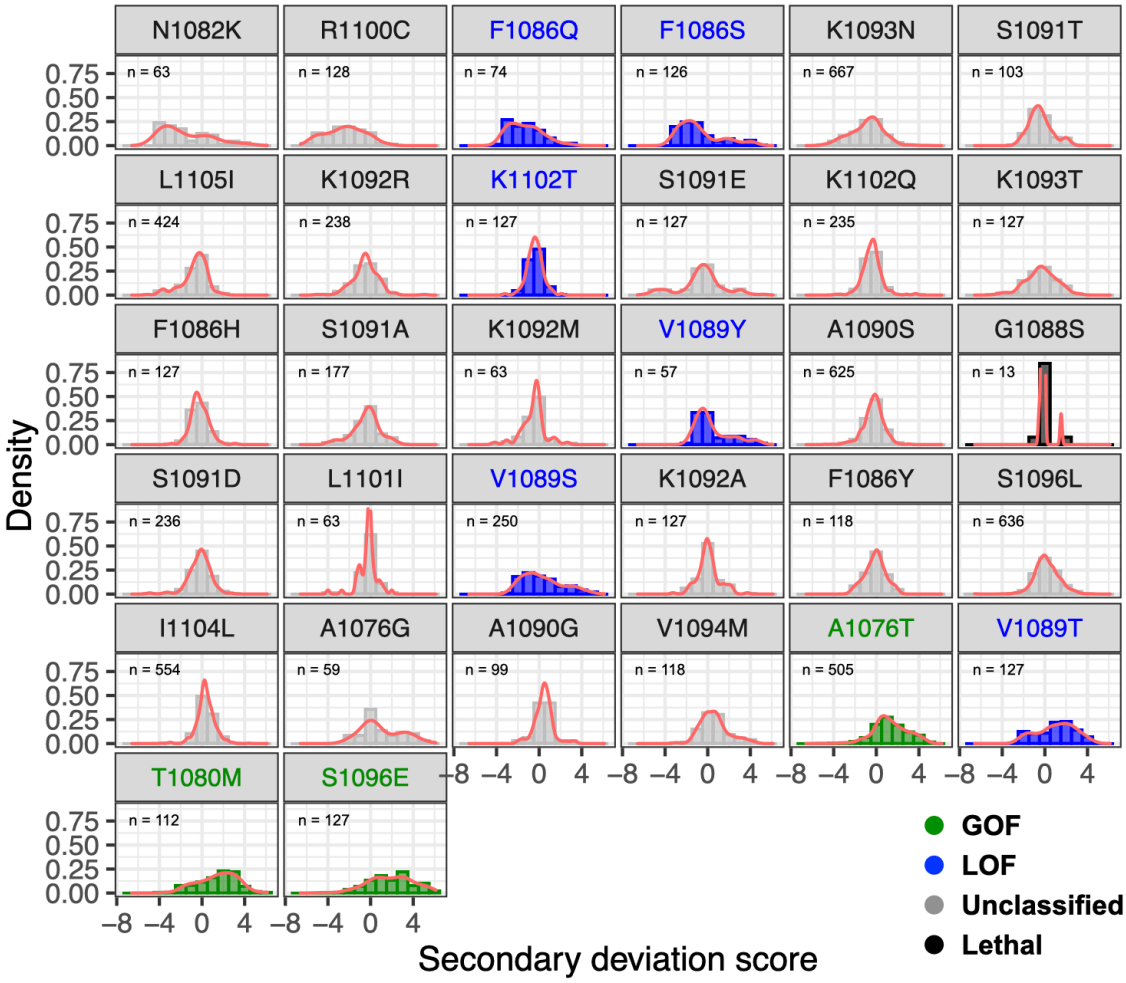

Figure S12. The density plots of secondary deviation scores of each substitution. We made density plots to display the distribution of secondary deviation scores for each substitution. The density plots were calculated of substitutions from nonrepetitive intermediate combinations across all haplotypes. The count of nonrepetitive intermediate combinations containing the substitution is shown in the upper left of each plot.

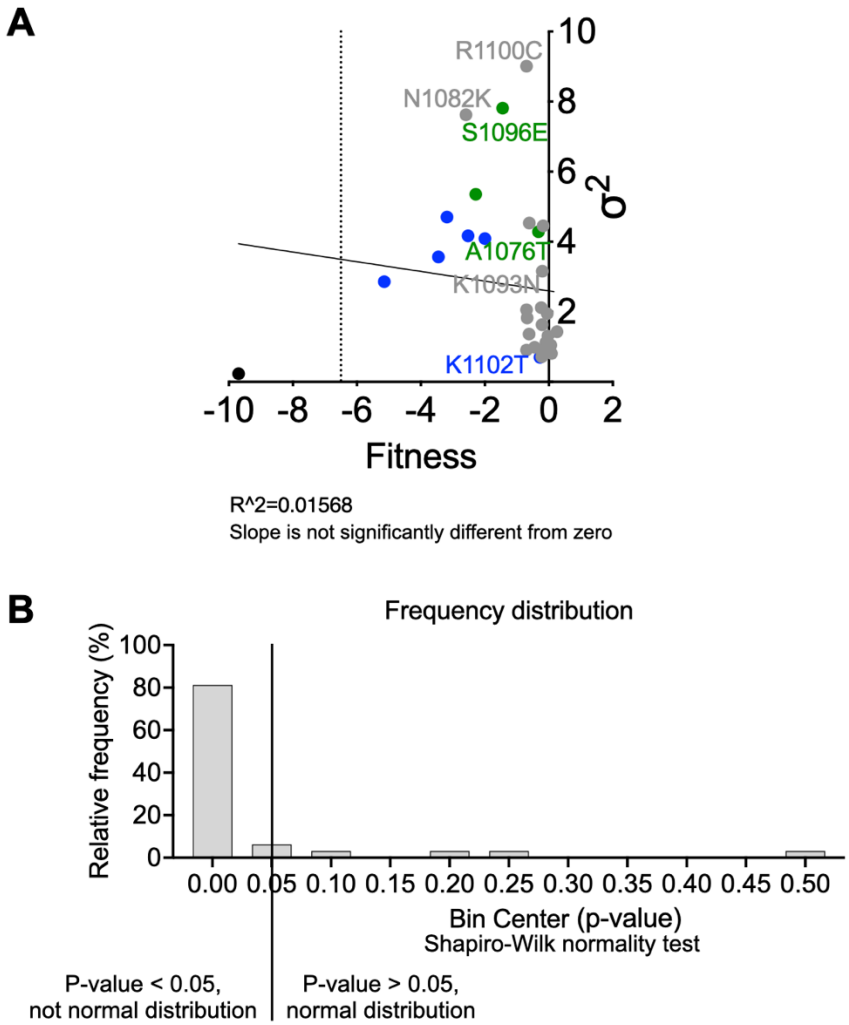

Figure S13. Slight but not significant negative correlation between σ^2 and fitness of substitutions. A. The correlation between the maximum likelihood estimate (σ^2) and the fitness of each substitution. Simple linear regression was applied ($y = -0.1384*x + 2.600$, $R^2 = 0.01568$). The slope is not significantly different from zero (P = 0.5101). **B**. The histogram of p-values from normality test. The density plots of secondary deviation scores have been tested whether they follow normal distribution by Shapiro-Wilk normality test. The null hypothesis of the test is the distribution follows normal distribution. Substitutions with P-value > 0.05 suggest their distributions are normal and P-value < 0.05 indicate their distributions do not follow normal distribution. ~80% of substitutions do not follow normal distribution.